Distribution: Restricted

Analysis of MERIS based global P-model GPP

Van Hoolst Roel, Else Swinnne, Colin Prentice

Study accomplished under the authority of ESA

January 2019

DISTRIBUTION LIST

Philippe Goryl, ESA-ESRIN
Fabrizio Niro, ESA-ESRIN

Else Swinnen, VITO
Roel Van Hoolst, VITO
Bruno Smets, VITO

Iain Colin Prentice, ICL
Keith Bloomfield, ICL
Wenjia Cai, ICL
Rebecca Thomas, ICL

Ivan Janssens, UA
Sara Vicca, UA
Manuela Balzarolo, CREAF

SUMMARY

This report describes the 10-daily two year (2007-2008) global P-model GPP outputs derived from MERIS fAPAR, AATSR Land Surface Temperature and ECMWF meteo data. This dataset is compared against similar Earth Observation (EO) products such as Copernicus Gross Dry Matter Productivity (GDMP) and the MODIS GPP.

In the first chapter of document, the three EO datasets are described. The second chapter describes the validation approach and methodologies. The third chapter contains the results and in the last chapter, general conclusions are drawn.

TABLE OF CONTENTS

LIST OF FIGURES

LIST OF TABLES

LIST OF ACRONYMS

AATSR	Advanced Along Track Scanning Radiometer
ATBD	Algorithm Theoretical Basis Documents
CCI	Climate Change Initiative
CEOS	Committee on Earth Observation Satellite
CGLS	Copernicus Global Land Service
DM	Dry Matter
DMP	Dry Matter Productivity
ECMWF	European Centre for Medium-Range Weather Forecasts
ENVISAT	Environmental Satellite
EO	Earth Observation
ESA	European Space Agency
FACE	Free-air concentration enrichment
FAO	Food and Agricultural Organization of the United Nations
fAPAR	Fraction of Absorbed Photosynthetically Active Radiation
GAUL	Global Administrative Unit Layer
GDMP	Gross Dry Matter Productivity
GPP	Gross primary production
LAI	Leaf Area Index
LCCS	Land Cover Classification System
LPV	Land Product Validation
LST	Land Surface Temperature
LUE	Light Use Efficiency
MEP	Mission Exploitation Platform
MERIS	MEdium Resolution Imaging Spectrometer
MODIS	Moderate-resolution Imaging Spectroradiometer
NetCDF	Network Common Data Form
NTSG	Numerical Terradynamic Simulation Group
PEM	Production Efficiency Models
R	Radiation
SPIRITS	Software for Processing and Interpreting Remote Sensing Image Time Series
VITO	Flemish institute for technological research
VPD	Vapour Pressure Deficit

CHAPTER 1 GLOBAL P-MODEL IMPLEMENTATION

1.1. DESCRIPTION OF P-MODEL GPP

The P model is fully derived and described by Wang et al. (2016a). Aspects of the underlying theory have been applied by Keenan et al. (2016) and Wang et al. (2016b). The P model possesses all of the following desirable attributes for a 'next-generation' primary production monitoring system:

- An explicit derivation from the FvCB model, and a clear relationship to a well-established functional form for stomatal behaviour – both elements required for a prediction of GPP.
- A representation of physiological CO_2 effects on photosynthesis that is consistent with both the FvCB model and results from FACE experiments.
- No distinctions among plant functional types and biomes (except for the difference between C_3 and C_4 plants), eliminating the need for spatial discontinuities induced by the use of a land-cover classification and look-up table.
- Demonstrated success in representing flux-derived GPP across different biomes at monthly time scales.

The model is extremely parameter-sparse, while achieving a fidelity to data comparable with or better than other models. This combination of simplicity with accuracy has been achieved through the development of theory that accounts for the observed environmental dependencies of the ratio (henceforth termed χ) of the leaf-internal (c_i) to ambient (c_a) partial pressures of CO_2 in C_3 plants; and the acclimation of photosynthetic parameters in space and time. Both aspects of the theory rely on eco-evolutionary optimality concepts to derive testable hypotheses, which in turn yield good agreement with observations from field measurements and field experiments.
Full details in TerrA-P_ATBDv2_I1.0.pdf (online at terra-p.vito.be).

1.2. GLOBAL P-MODEL IMPLEMENTATION

A global test dataset at 1 km was generated for the years 2007 – 2008. Orginally two versions of the P-model are available: a C3 and C4 model. But in this global implementation, only C3 outputs are generated.

The implementation of the P-model on global data includes a number of steps:

- Revision of the P-model code to operate on 2-D arrays
- Preparation of the global input rasters
- Testing & output analyses on a subsampled dataset
- Set-up of a global full resolution software chain

1.2.1. REVISION OF THE P-MODEL CODE TO OPERATE ON 2-D ARRAYS

The initial P-model code was revised by ICL. Following adjustments were made:

- A separate Python file with the majority of the model component functions

- A separate Python file with the uncertainty calculation procedures
- Each of these functions is developed to work on 2-D arrays
- Initially these 2-D arrays were time series of point location data. But as the P-model is location nor time dependent, also 2-D arrays derived from raster files can be fed into the algorithm

This prototype algorithm code was uploaded to a private repository on the VITO GIT server.

1.2.2. PREPARATION OF THE GLOBAL INPUT RASTERS

Following input global datasets were used to produce MERIS based global GPP estimates with the P-model:

Table 1: Input datasets used in the global GPP estimates with the P-model.

Parameter	Dataset	Source	Resolution	Timestep	Data format
Daily incoming radiation [kJ/m2/d]	ECMWF	VITO via Meteogroup	0.25°	10-daily average	ENVI image
Average water vapour pressure [hPa]	ECMWF	VITO via Meteogroup	0.25°	10-daily Average	CSV
fAPAR [-]	ENVISAT - MERIS	VITO EO portal	1/112°	10-daily max value	ENVI image
LST [°C]	ENVISAT - AATSR	GlobTemp project	Non-gridded	Daily	NetCDF per orbit

The P-model requires as input equally shaped arrays for fAPAR, LST and meteo data. For image processing, these arrays are the input images for a specific timestep. Hence all inputs should be harmonized to a 1km fixed grid at a 10-daily timestep (as defined in the product specification survey). The grid is defined as follows:

Table 2: Geospatial parameters defining the 1 km grid.

```
columns      : 40320
rows         : 14673
ref. system  : Geographic Lat/Lon
ref. units   : deg
unit dist.   : 1
min. X       : -180.004464
max. X       : 179.995536
min. Y       : -56.0044643
max. Y       : 75.0044643
resolution   : 0.00892857143
```

All inputs and thus also the outputs are generated at a 10-daily" timesteps. This "dekadal" periodicity is defined such that each month contains three timesteps or "dekads":

- Day 1 – 10: dekad 1
- Day 11 – 20: dekad 2
- Day 21 – end of month: dekad 3

Below, we further describe the dataset specific preprocessing steps.

→ Preprocessing meteo data

- The "Average Water Vapour Pressure" is obtained via Meteogroup in CSV files, containing for each 0.25° grid cell the respective values. These CSV files are transformed to georeferenced images and resampled to the 1km TerrA-P grid.
- The "Daily Incoming Radiation" data is already available at 10-daily images via the MARSOP and Copernicus Global Land Service. These images at 0.25° are resampled to the 1 km Terra-P grid.

→ Preprocessing fAPAR data

The MERIS fAPAR data was retrieved via the VITO platform (vito-eodata.be). These ENVISAT MERIS S10 or "EM10" are near-global, 10-daily composite images of the Fraction of Absorbed Photosyntheticly Active Radiation (fAPAR) taken from ENVISAT MERIS Level 2 Reduced Resolution data. The temporal compositing is done by taking the maximum fAPAR within the 10-daily period. In particular, the standard fAPAR band and rectified Near-infrared and Red reflectance bands are used and filtered, using the L2 flags and a static mask, and mosaiced onto a grid of 112 pixels per degree, for easier comparison of SPOT-VEGETATION and MetOp-S10.

To eliminate spatial and temporal gaps and to eliminate outliers in the data, a gap-filling and smoothing procedure was applied on the 2007 – 2008 time series. This gap-filling procedure For this the SPIRITS software (spirits.jrc.ec.europa.eu) was used. A Swets smoothing procedure was selected (Swets et al., 1999). The parameters are described below. The effect on pixel time series is shown in Figure 1. The pixels with "no data" in winter time in the northern hemisphere are filled by means of interpolation. The global effect for April 2007 is shown in Figure 2. Many regions with no-data at northern altitudes in the winter/early spring have an interpolated gap filled value in the smoothed version. These values are however mostly reset to GPP=0 g C/m2/day by the P-model as their Land Surface Temperature (LST) often drops below 0° C.

Table 3: SPIRITS smoothing parameters for Swets smoothing applied on the global MERIS fAPAR.

```
-----------------
SMOOTH - PRE:          Preliminary elimination of suspect observations in each pixel profile:
-----------------
PreMaxTop    = 0.40    Local maxima if difference to both neighbours exceeds PreMaxTop                    (def=1000000 => Skip)
PreMaxGap    = 0       Keep gaps longer than this nr. of DAYs, reset them to Ymin (p24), presumably SNOW/POLAR WINTER      (def=0     => Skip)
PreMaxGapMsk  = W:\TerraP\MERIS\cgls\ref\msk\SNOWmsk      Optional BYTE SnowMask-IMG: only apply PreMaxGap for pixels with SnowMask-values > 0 (land susceptible
to snow/ice).
-----------------
SMOOTH - Method 2:       SWETS
-----------------
                 SWETS regression weights for different observations in pixel profile
SwWmax      = 1.5      for local maxima                                        [def=1.5]
SwWmin      = 0.005     for local minima                                       [def=0.005]
SwWplane     = 1.0      for planes (same value as 2 neighbours)          [def=1.0]
SwWslope     = 0.5      for all others in regular profile                [def=0.5]
SwWedge      = 0.5      for Left/Right edge point in profile                   [def=0.5]

                 SWETS regression parameters
SwWinR      = 50       Length in DAYS of regression  window: regression parms (A,B) calibrated with these points [2-201, def=50]
SwWinC      = 50       Length in DAYS of combination window: regression applied to these points           [2-201, def=50, min=SwWinR]
SwCI       = 0       Confidence Interval in %, for outlier correction with CHI2-test [def=95%] - Skip this test with SwCI=0 (or 100).
-----------------
-----------------
SMOOTH - POST:          A posteriori adaptations of smoothed profiles (default values are 0 = Skip adaptations).
-----------------
PostOver     = 0       Remove some of the apparent over-estimations[0/1]. DANGEROUS, BEST SKIP!
                              Only allowed for SWETS and MEAN with MuInterpol=1.
                 For BISE, WHITTAKER and MEAN with MuInterpol=0, PostOver is always reset to zero (=skip).
PostUnder    = 1       Reset estimates which are below the "original" (PRE-Smoothed) value [0/1]
PostMax      =-1       Reset all estimates > PostMax to this PostMax (0=skip test, -1=use each pixel's original maximum)
```

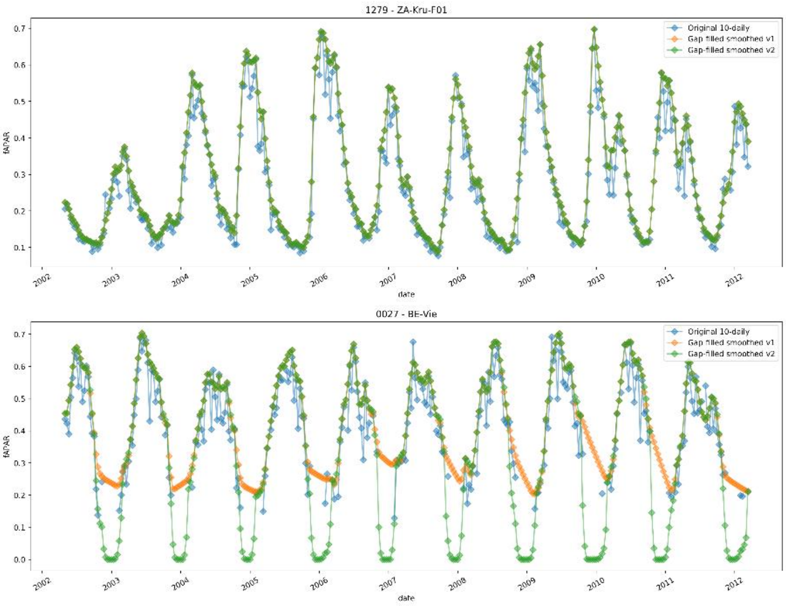

Figure 1: Original (blue) time series of fAPAR for the period 2002-2012, Swets smoothed version 1 (orange, that interpolates data gaps) and a smoothing version (green, that introduces a base fAPAR value of 0.0 for data gaps of >40 days) for a site in South Africa (upper) and Belgium (lower).

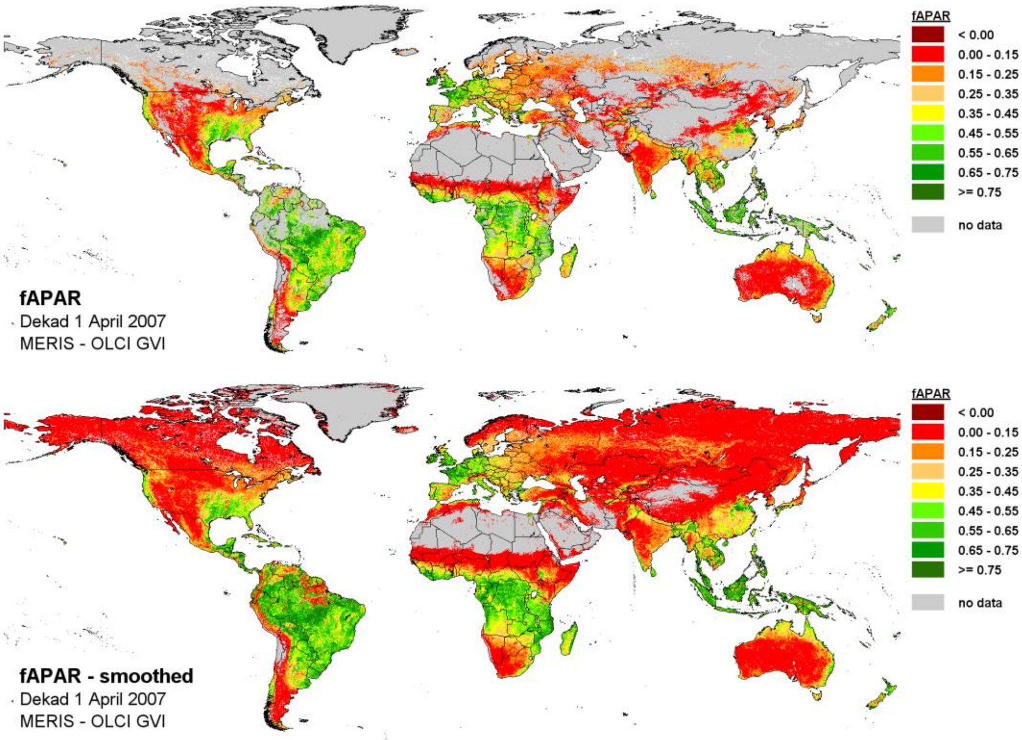

Figure 2: Original and smoothed MERIS fAPAR for April 2007. In the smoothed version, no data pixels are filled by means of interpolation with neighbouring observations in time.

→ Preprocessing LST

The orginal AATSR LST dataset was retrieved via the GlobTemp project (globtemperature.info). The level-2 (AATSR_LST_2) was downloaded for 2007 & 2008. The original NetCDF format contains orbital data, with a layer containing the actual values, two layers describing the longitude and latitude of the observation and a number of quality layers. This dataset was preprocessed as follows:

- Import of all orbital data per day. Based on the quality layers, only daytime and cloudfree pixels are retained.
- The remaining pixels are mapped onto the 1km reference grid. For pixels with multiple observations, the selection is based on the smallest satellite zenith angle ("satze" layer). The result are daily global mosaics.
- These daily data is further temporally aggregated to 10-daily composits, based on the mean value composit, i.e. the average value over the 10-day periods.
- The resulting set of 10-daily images are further smoothed with a second difference Whitakker (elaborated in Eilers, 2003) smoothing algorithm to obtain a gap-filled and smoothed 10-daily dataset. Parameter details in Table 4. The effect of the smoothing on two sites in Belgium and South Africa is shown in Figure 3. The global effect is presented in Figure 4.

Table 4: Whitakker parameters.

```
lmbda                   = 1
passes                  = 3
dokeepmaxima            = True
minimumdatavalue        = None
maximumdatavalue        = None
aboutequalepsilon       = 0.01
```

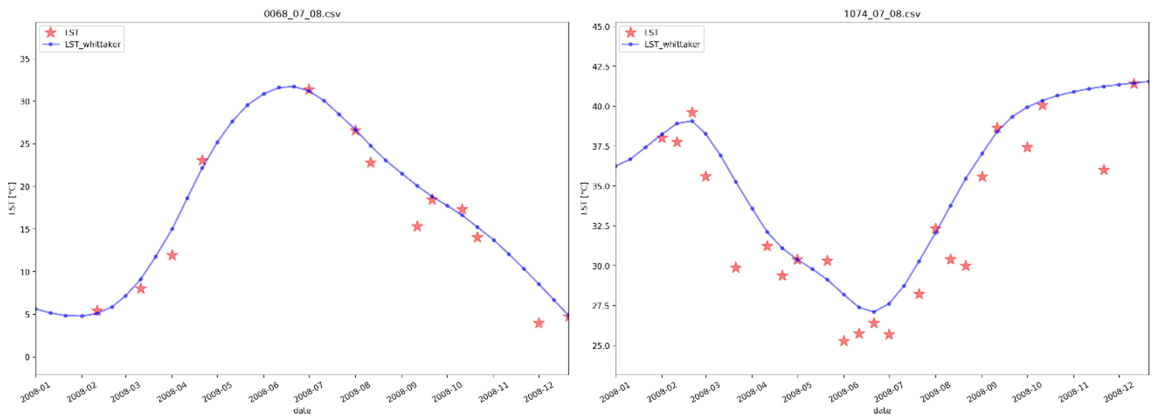

Figure 3: Effect of Whitaker smoothing on raw daily LST data for a site in Belgium, Brasschaat forest (left) and South Africa, Kruger Savanna (right). The red stars are the 10-daily composited values, the blue line is the fitted curve and the blue points are the retrieved smoothed 10-daily values.

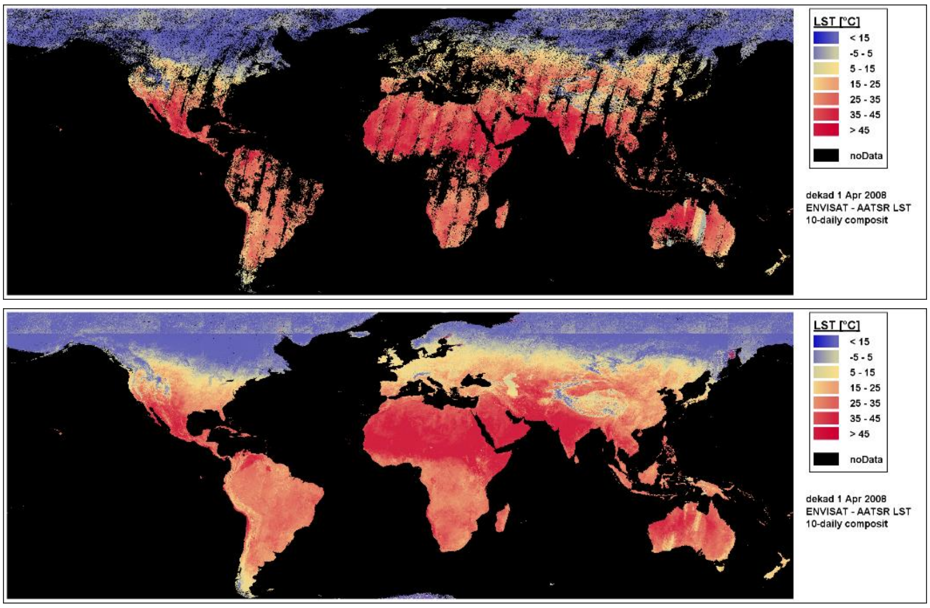

Figure 4: Original (upper) and smoothed and gap-filled global 1km LST [°C] for the first dekad of april 2008. The stripe in the northern hemisphere is caused due to day/nighttime restrictions of the sensor.

1.2.3. TESTING & OUTPUT ANALYSES ON A SUBSAMPLED DATASET

All initial developments and testing of the global processing chains were done on a subsampled global input dataset. From the original 1 km rasters, a systematic subsampling was done by extracting only the pixels each 21th row/column. This systematic subsampling allows fast processing and analysis while keeping the global spatial landscape patterns. The resulting images are 1920 x 698 pixels, which is about 1.3 MB for a Byte image. This “thinned” dataset was further used to analyse the global outputs and compare against similary subsampled Copernicus and MODIS datasets.

Important remark:

- The 10-daily LST observations are based on a “mean”-compositing rule, taking the average over all daily observations in the 10-day window. These values are further smoothed and gap-filled to get a continuous time series over the 36 dekads throughout the year. Main question: How do we treat the uncertainties, which are linked with the original “daily” observations?
- This issue is still unclear. There have been discussions internally and with LST experts, but without a clear consensus if these uncertainties can be propogated in the preprocessing and model run. So for now, we do not propagate the LST uncertainties in the final GPP product.
- The output per pixel uncertainties are thus based on the model uncertainties and input values, not on input uncertainties.

1.2.4. SET-UP OF A GLOBAL FULL RESOLUTION SOFTWARE CHAIN

A global software chain was developed and embedded in the Mission Exploitation Platform (MEP) at VITO’s server. The chain splits all input in tiles (10°x10°) to ease parallelization. This software chain was used to produce the 1 km global output GPP images.

CHAPTER 2 DESCRIPTION OF BENCHMARK EO GPP DATASETS

2.1.1. COPERNICUS GLOBAL LAND SERVICE DMP

Description:
The DMP product of the Copernicus Global Land Service (CGLS) is based on the Light Use Efficiency (LUE) approach, first formulated by Monteith (1972). He stated that the vegetation growth is completely defined as the part of the incoming solar radiance that is used for photosynthesis and which is absorbed by the plants (APAR, [$kJ_{AP}/m^2/d$]) and a number of conversion efficiency factors.
The Version 2 of GDMP and DMP product of the CGLS is computed with the following Monteith variant (see Table 5):

$$GDMP = R.\varepsilon_c.fAPAR.\varepsilon_{LUE}.\varepsilon_T.\varepsilon_{CO2}\ [.\varepsilon_{RES}]$$
$$DMP = R.\varepsilon_c.fAPAR.\varepsilon_{LUE}.\varepsilon_T.\varepsilon_{CO2}.\varepsilon_{AR}[.\varepsilon_{RES}]$$

Table 5: Individual terms in the Monteith variant used for Global Land service GDMP/DMP. All terms are expressed on a daily basis. Details are described in the Copernicus DMP ATBD (Swinnen et al., 2018)

TERM	*MEANING*	*VALUE RANGE*	*UNIT*
GDMP	Gross Dry Matter Productivity	0 – 640	kgDM/ha/day
DMP	Dry Matter Productivity	0 – 320	kgDM/ha/day
R	Total shortwave incoming radiation (0.2 – 3.0µm)	0 – 320	GJ_T/ha/day
ε_c	Fraction of PAR (0.4 – 0.7µm) in total shortwave	0.48	J_P/J_T
*f*APAR	PAR-fraction absorbed (PA) by green vegetation	0.0 ... 1.0	J_{PA}/J_P
ε_{LUE}	Light use efficiency (DM=Dry Matter) at optimum	Biome-specific	$kgDM/GJ_{PA}$
ε_T	Normalized temperature effect	0.0 ... 1.0	-
ε_{CO2}	Normalized CO_2 fertilization effect	0.0 ... 1.0	-
ε_{AR}	Fraction kept after autotrophic respiration	0.5	-
ε_{RES}	Fraction kept after omitted effects (drought, pests...)	1.0	-

Relation between Gross Primary Production (GPP) and Gross Dry Matter Productivity (GDMP)
GDMP, or Gross Dry Matter Productivity, represents the overall growth rate or dry biomass increase of the vegetation, expressed in kilograms of dry matter per hectare per day (kgDM/ha/day). GDMP is directly related to GPP (Gross Primary Productivity, in gC/m²/day), but its units are customized for agro-statistical purposes.

$$1\ kgDM/ha/day = 1000\ gDM/ha/day = 0.1\ gDM/m^2/day$$

According to Atjay et al. (1979), the efficiency of the conversion between carbon and dry matter is on the average 0.45 gC/gDM. So GPP and GDMP only differ by a constant. In practice, to scale GDMP to NPP following calculation should be done:

$$GPP\ [gC/m_2/day] = GDMP\ [kgDM/ha/day] * 0.45 * 0.1$$

Input data:

Meteodata

Up till 2014, the global meteo data were delivered by MeteoConsult in the frame of MARSOP3, in the form of daily CSV-files, providing for each "grid-cell" (at 0.25° resolution) the values of all standard meteorological variables. Basically, all daily data are "operational forecasts for the next 24 hours" derived from ECMWF (ERA-Interim for the years 1989-2008). Copernicus GL service adopted the retrieval of the global meteorological data from MeteoConsult in dito format.
The ECMWF climate data are used in different parts of the DMP algorithm:

- ***Radiation*** as basic input for the Monteith model.
- ***Temperature*** (daily minimum/maximum) in the temperature dependency for photosynthesis.

fAPAR

fAPAR corresponds to the fraction of photosynthetically active radiation absorbed by the green elements of the canopy. It depends on canopy structure, vegetation element optical properties and illumination conditions. The DMP uses the CGLS fAPAR Version 2 product, being produced 10-daily and at 1 km resolution. This method capitalizes on the development and validation of already existing products: CYCLOPES version 3.1 and MODIS collection 5, and the use of neural networks (Verger et al., 2008). The fAPAR Version 2 is described in detail in the ATBD (GIOGL1_ATBD_FAPAR1km-V2, found online at land.copernicus.eu).

Land cover information

The DMP v2 uses biome specific Light Use Efficiency (LUE) values. The information on the global distribution of land cover types comes from the ESA CCI Land Cover Map (epoch 2010), which was derived from ENVISAT-MERIS and SPOT-VGT imagery of the period 2008-2010. The land cover classes are based on the UN Land Cover Classification System (LCCS).

2.1.2. MODIS GPP

Description:

MODIS provides GPP/NPP data from the Numerical Terradynamic Simulation Group (NTSG) of the University of Montana (http://www.ntsg.umt.edu/project/mod17). The MOD17 algorithm, described in detail by Running et al. (1999), Heinsch et al. (2003), Zhao et al. (2005) is a satellite based Production Efficiency Model (PEM) of the form of Montheith (1972), which suggests that productivity of annual crops under well-watered and fertilized conditions is linearly related to the amount of absorbed Photosynthetically Active Radiation (APAR). The translation of APAR to an actual productivity estimate (Gross Primary Productivity, GPP) is conducted via a conversion efficiency parameter, ε, which varies by vegetation type and climate conditions. The GPP is reduced at yearly base with the maintenance and growth respiration derived from allometric relationships linking daily biomass and annual growth of plant tissues to satellite-derived estimates of leaf area index (LAI, MOD15) to result in the NPP.

Input data:

The MOD17 algorithm uses the Fraction of Photosynthetically Active Radiation (fAPAR) and Leaf Area Index (LAI) derived from the MODIS MOD15 LAI/FPAR data product. Temperature, incoming solar radiation, and vapor pressure deficit (VPD) are derived from a meteorology dataset. Meteorology datasets used by various versions of the MOD17 algorithm include products from the NASA Global Modeling and Assimilation Office and the NCEP/NCAR Reanalysis II. The MODIS MCD12Q1 data product is used as a land cover classification.

CHAPTER 3 QUALITY ASSESSMENT APPROACH

3.1. GENERAL APPROACH

The objective of this quality assessment is to gain insights in the relation between the global P-model GPP estimates and existing EO products. This is not considered as a hard validation of the P-model GPP as each of these datasets have their own methodology with corresponding assumptions, limitations and input data.

No standard procedure exists to assess the performance of EO-derived GPP products. Therefore, a procedure adapted from the guidelines, protocols and metrics defined by the Land Product Validation (LPV) group of the Committee on Earth Observation Satellite (CEOS) for the validation of satellite-derived land products was used. These are:

(1) Visual inspection: The time series of GPP and GPP uncertainty maps are visually inspected.

(2) Product completeness: Analysis of the number of valid observations in both space and time.

(3) Global EO intercomparison:

a. *Spatial distribution of the GPP estimates*: global maps of metrics expressing the similarity and difference between the 10-daily P-model GPP images and MODIS and Copernicus GPP.
b. *Histograms: Value* Frequency distributions of GPP estimates were computed over biomes. An aggregated version of the ESA CCI land cover map was used for this purpose (section 3.3).
c. *Scatterplots* between the TerrA-P GPP product and the reference products (MODIS, Copernicus) were produced at a global scale and per land cover type.
d. *Temporal variation per biome*: Globally or per contintent biome specific aggregated values are plotted in time and compared with the other EO products.

(4) Local Accuracy assessment

a. *Direct validation*: The FLUXNET in situ measurements can be considered as ground truth reference data. Scatterplots and validation metrics are used to compare the relation between the P-model GPP and FLUXNET GPP. The same analysis is done for CGLS and MODIS, to compare the accuracies of the datasets.

3.2. Statistical measures

3.2.1. The coefficient of determination (R^2)

The coefficient of determination (R^2) indicates agreement or covariation between two data sets with respect to a linear regression model. It summarizes the total data variation explained by this linear regression model. The result varies between 0 and 1 and higher R^2 values indicate higher covariation between the data sets. In order to detect a systematic difference between the two data sets, the coefficients of the regression line should be used.

$$R^2 = \left(\frac{\sigma(X,Y)}{\sigma(X) \cdot \sigma(Y)}\right)^2$$

With $\sigma(X)$ and $\sigma(Y)$ the standard deviation of X and Y and $\sigma(X,Y)$ the covariation of X and Y. The R^2 is provided only together with the scatterplots, because it allows a quantitative interpretation of the scatterplots.

3.2.2. Geometric mean regression

Model I regression models (e.g. Ordinary Least Squares) are appropriate for predicting one data set out another and one data set is assumed error-free. This is not the case when comparing two similar data sets of remote sensing images, because both are subjected to noise. In this case, model II regression models are more suited. Different regression models II exist, such as the geometric mean (GM), orthogonal and OLS bisector regression models.
The difference between the models is in the way the errors are minimized

- OLS minimizes the sum of the squared vertical distances (errors on Y) from the data points to the regression line
- GM minimizes the sum of the products of the vertical and horizontal distances (errors on Y and X)
- Orthogonal regression minimizes the sum of the squared perpendicular distance from the data point to the line (errors on Y and X)
- OLS bisector regression bisects the angle between the Y on X OLS regression line and the X on Y OLS regression line.

Each of the model II regression analysis methods has its merits and deficiencies. Here, the GM regression model was used because of its simplicity.

3.2.3. THE ROOT MEAN SQUARED ERROR (RMSE)

The Root Mean Squared Error (RMSE) measures how far the difference between the two data sets is from 0 and is defined as

$$RMSE = \sqrt{\frac{1}{n}\sum_{i=1}^{n}(X_i - Y_i)^2}$$

The RMSE includes both systematic and unsystematic differences and is a widely used difference measure, but it lacks the differentiation between systematic and random error. However, based on our experience, it provides a better differentiation (especially spatially) compared to the MSD, and it is easier to interpret (same scale as inputs).

3.2.4. THE MEAN SQUARED DIFFERENCE (MSD)

The mean squared difference (MSD) is defined as

$$MSD = \frac{1}{n}\sum_{i=1}^{n}(X_i - Y_i)^2 = \frac{1}{n}SSD$$

It can be further partitioned into the systematic mean product difference (MPD_s) and the unsystematic mean product difference (MPD_u).

$$MPD_u = \frac{1}{n}\sum_{i=1}^{n}\left(\left|X_i - \hat{X}_i\right|\right)\left(\left|Y_i - \hat{Y}_i\right|\right)$$

With $\hat{X}_i$ and $\hat{Y}_i$ calculated using the GM regression line and n the number of samples. Then, $MPD_s = MSD - MPD_u$

3.3. REGIONAL/BIOME ASSESSMENT

The land cover specific analyses are done for 12 biomes. But in each analysis, only results for specific biomes of the most relevant findings are published in this report. A reclassified ESA CCI map is used as stratification. Table 6 shows the legend of the original ESA CCI and the derived merged classes. Mixed classes and classes with low vegetation density are not included in the analysis. Figure 5 shows a global map of the biomes with the original legend and a map showing only the six biomes used in the analyses of this report.

Table 6: The original (left) and rescaled (right) ESA CCI land cover classes.

CCI class id	CCI class name	Rescaled class id	Rescaled class abbr	Rescaled class name
0	No Data	0	NOD	NoData
10	Cropland:rainfed	1	CRO	Cropland-Rainfed
11	Cropland: rainfed (Herbaceous)			
12	Cropland: rainfed (Tree/Shrub)			
20	Cropland: irrigated or post-flooding			
30	Mosaic Cropland(>50%)/ Natural Vegetation	2	MCN	Mosaic-Cropland-Natural
40	Mosaic Cropland(<50%)/ Natural Vegetation			
50	Tree Cover: Broadleaved Evergreen (>15%)	3	BEF	Broadleaved-Evergreen-Forest
60	Tree Cover: Broadleaved Deciduous (>15%)	4	BDF	Broadleaved-Deciduous-Forest
61	Tree Cover: Broadleaved Deciduous (>40%)			
62	Tree Cover: Broadleaved Deciduous (15-40%)			
70	Tree Cover: Needleleaved Evergreen (>15%)	5	NEF	Needleleaved-Evergreen-Forest
71	Tree Cover: Needleleaved Evergreen (>40%)			
72	Tree Cover: Needleleaved Evergreen (15-40%)			
80	Tree Cover: Needleleaved Deciduous (>15%)	6	NDF	Needleleaved-Deciduous-Forest
81	Tree Cover: Needleleaved Deciduous (>40%)			
82	Tree Cover: Needleleaved Deciduous (15-40%)			
90	Tree Cover: Mixed leaf type (broad- and needleleaved)	7	MIX	Mixedleaf-Mosaic-Tree-Shrub-Herbaceous
100	Mosaic Tree Shrub(>50%)/Herbaceous			
110	Mosaic Tree Shrub(<50%)/Herbaceous			
120	Shrubland	8	SHR	Shrubland
121	Evergreen Shrubland			
122	Decidous Shrubland			
130	Grassland	9	GRA	Grassland
140	Lichens and Mosses	10	SPR	SparseVegetation
150	Sparse Vegetation (<15%)			
152	Sparse Shrub (>15%)			
153	Sparse Herbaceous (<15%)			
160	Tree Cover: Flooded fresh/brakish	11	FLD	Flooded-Tree-Shrub-Herbaceous
170	Tree Cover: Flooded saline			
180	Shrub or Herbaceous: Flooded fresh/saline/brakish			
190	Urban Areas	10	SPR	SparseVegetation
200	Barea Areas			
201	Consolidated Bare Areas			
202	Unconsolidated Bare Areas			
210	Water bodies	12	WAT	Waterbodies
220	Permanent snow and Ice	13	SNO	PermanentSnowAndIce

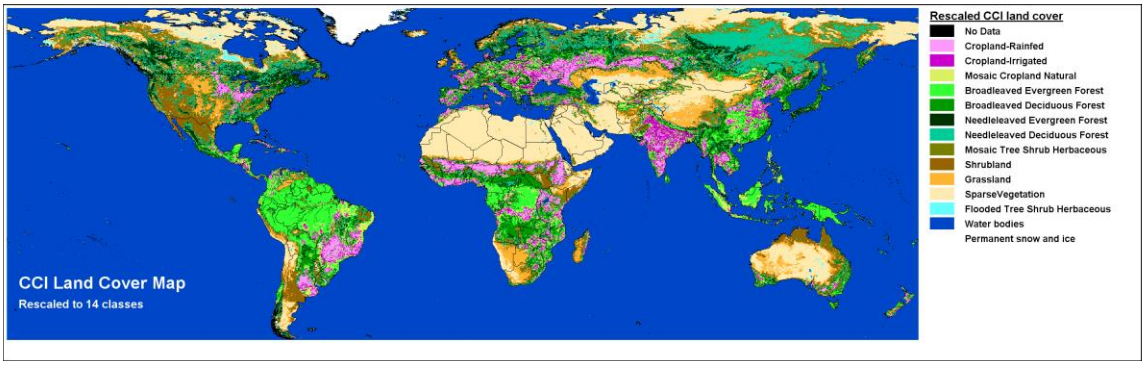

Figure 5: Original and rescaled ESA CCI land cover map.

Regional analyses are done on continental and regional scale. For this, a stratification is based on the GAUL (Global Administrative Unit Layer) of FAO. The figures below indicate the continental and regional boundaries used in further analyses.

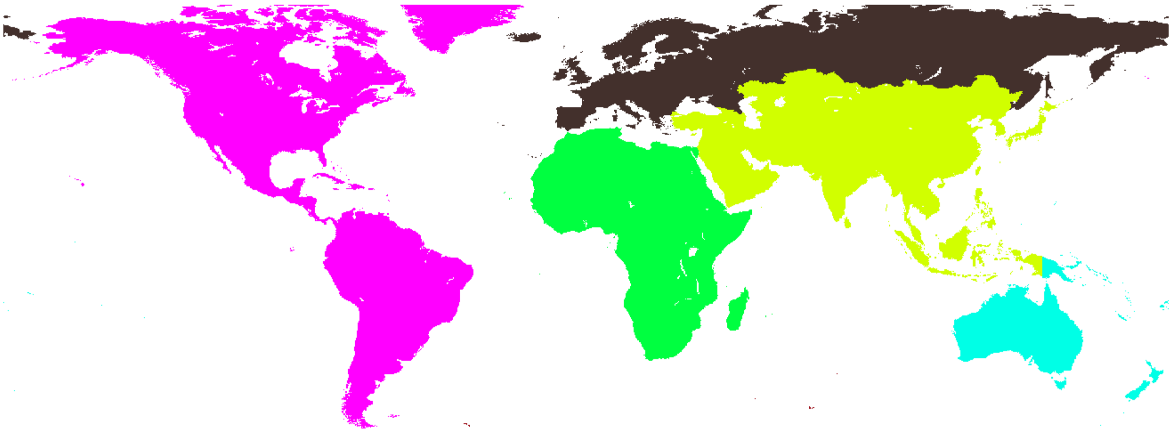

Figure 6: Continental units used in the analyses.

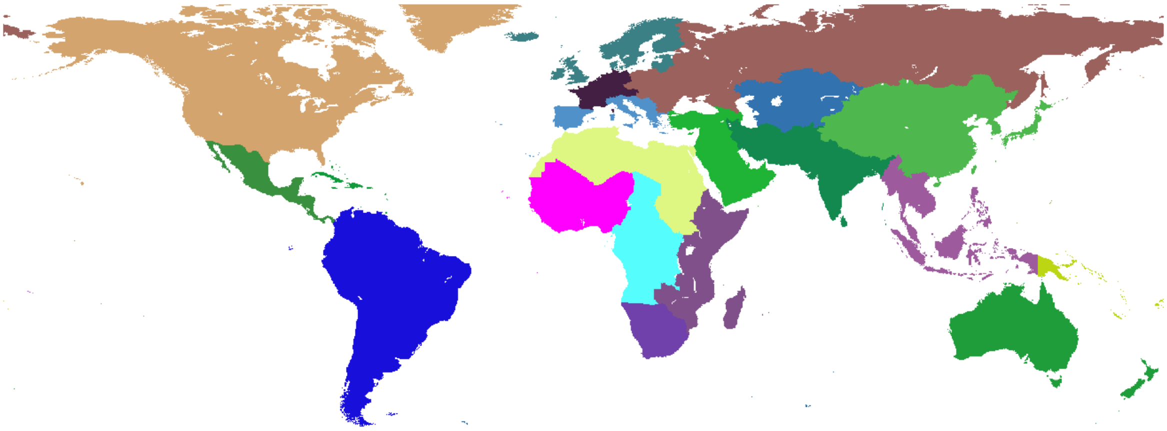

Figure 7: Regional units used in the analyses.

CHAPTER 4 RESULTS

4.1. GENERAL VISUAL INSPECTION

In this first part, we describe our first findings when visualy inspecting the output maps produced by the P-model on global fAPAR (MERIS) and LST (AATSR) data. These maps were also sent for inspection to the project partners and ESA. Their remarks are incorporated in the findings on the next page. In the remaining part of the chapter, an in-depth analysis of the global GPP estimates is done by comparing it with two EO datasets: Copernicus DMP and MODIS GPP.

Description on color scaling:

Figure 8 shows the global P-model output maps for GPP and GPP uncertainties for 4 periods in the year 2008: January, April, July and October. GPP values are scaled from **brown (0)** to **green (>10)** g C/m2/day. Three output flags indicate which input data was missing: "**missing_meteo**" (light grey), "**missing_lst**" (blue) and "**missing_fAPAR**" (black). The order of flagging is "missing_meteo", then remaining valid pixels are flagged with "missing_lst", and further masked with "missing_fapar". The pixels that have all input values are fed into the model and an output is given for GPP and GPP uncertainty. If the model fails to give either a GPP or GPP uncertainty value, the pixels are flagged with the magenta color (**no_data**).

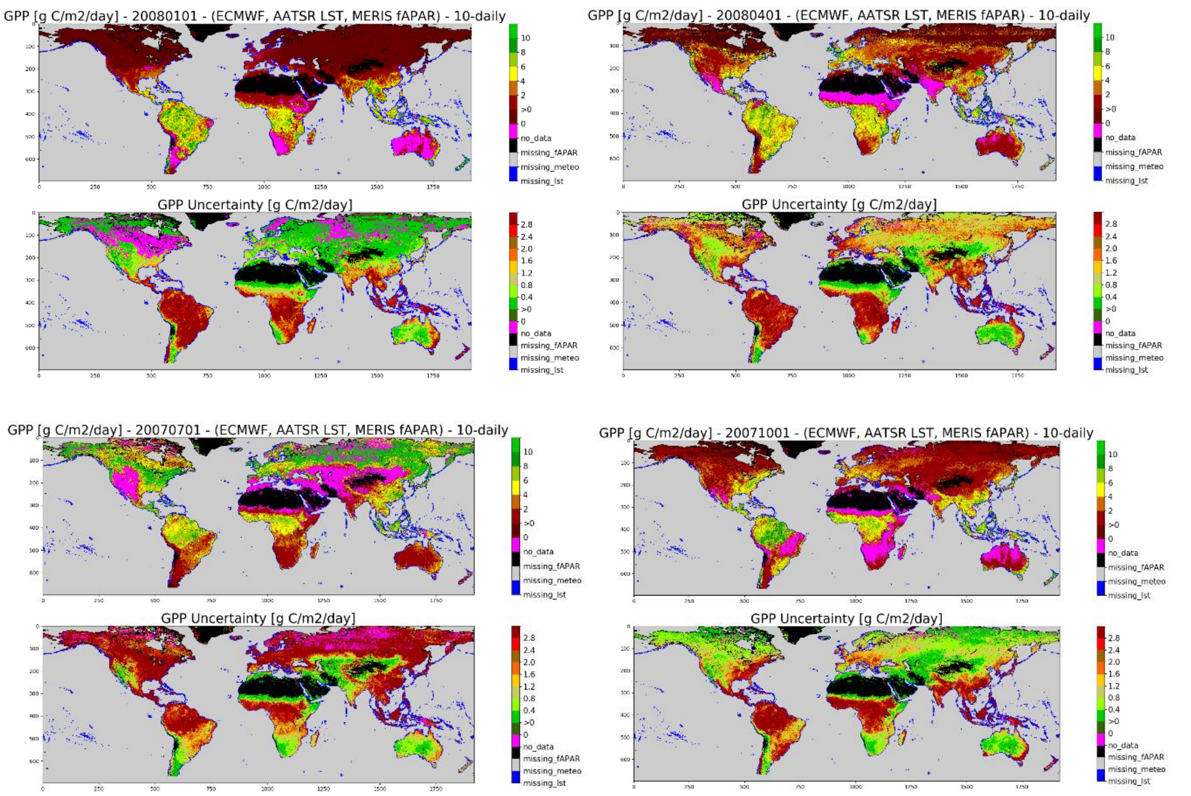

Figure 8: Seasonal snapshots (January, April, June, October) of global ENVISAT based GPP, calculated with the P-model.

First findings:

- The meteo data is only available for the land surfaces. Because of the difference in original resolution (0.25°) and 1 km LST/fAPAR, the borders of the oceans and water bodies are further masked with missing LST. An additional land cover mask could be used to discriminate the land from the sea pixels.
- Due to the use of gap-filled and smoothed LST values, the LST inputs are mostly available for all seasons and regions. (See Figure 4 which shows global original and smoothed LST).
- fAPAR data is not available over non-vegetated areas such as in the Sahara desert, middle east, Gobi desert and Greenland.
- It occurs that the model either gives GPP outputs when no uncertainties can be estimated, or the opposite way.
    - This has to be further investigated by the model developers.
- The C3 version of the model fails to provide GPP values ("no_data") for sparsely vegetated areas, e.g. inner Australia (January/October), Sahel (April), Great Basin – US (July),…
    - This is probably caused by too high LST values. In sparsely vegetated areas, the LST estimates are largely based on soil temperatures, rather then on vegetation canopy temperatures. This can result in extreme values (>45°C) which cause the C3 version of the P-model to produce model errors as it can't deal with these extremes. This is currently one of the major challenges when using LST data in the model temperature component.
    - These spatial patterns however are in agreement with the global C4 vegetation pattern. This C4 version of the model can deal with such extreme temperature values and should be used on these areas to calculate the GPP.
- There is a seeming artificial horizontal boundary in the northern regions in the April map. This is further propagated from the LST maps (day/night . (see Figure 4).
- The remaining GPP values shows seasonal and spatial patterns which are in agreement with our first intuitions.

4.2. Product completeness

Figure 9 shows the percentage of missing GPP values from January 2007 till December 2008 for the 1km 10-daily ENVISAT (MERIS fAPAR & AATSR LST) based GPP. Distinct spatial patterns are visible:

- Regions with >50% missing values over non-vegetated regions (e.g. Sahara, Middle East, Gobi desert, Great Basin, regions in Australia,…)
    - Explanation: For some of these regions, no fAPAR values were available, such as the Sahara or Greenland. For other regions (e.g. Grean Basin, inner Australia,…), the model doesn't provide a GPP estimate if the LST values are too high.
- In the northern regions, regions have between 0-25% of missing values. This is caused by the limited availability of observations in winter time. Two distinct horizontal boundaries are visible, probably due to day/nighttime restrictions of the AATSR LST and Solar Zenith Angle restrictions of the MERIS fAPAR.

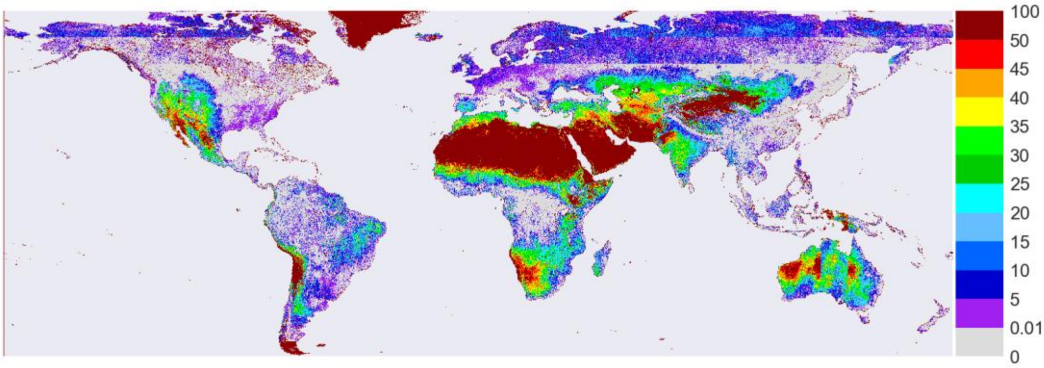

Figure 9: Spatial continuity (% missing values) of the 10-daily 1km ENVISAT (MERIS fAPAR & AATSR LST) based GPP in the period 2007-2008.

Figure 10 shows the temporal profile of the percentage of valid GPP pixels over land. The amount of valid observations range from +- 89 % (June/July) till 94 % (January/February). The order of magnitude seems ok. But the seasonal pattern is remarkable. One would expect least valid observations in winter time in the northern hemisphere, and most valid observations in global summer time. This unusual behavior is probably caused by the several masked pixels over sparsely vegetated areas due to extreme LST values in summer time.

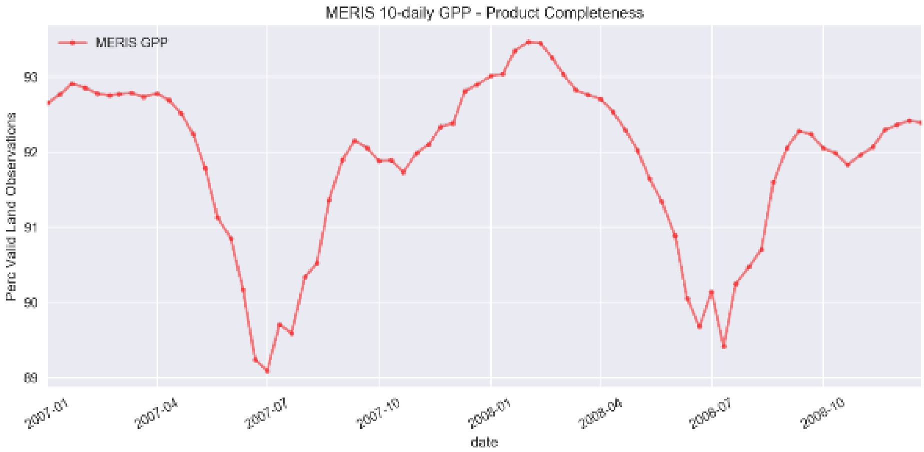

Figure 10: Analysis of the percentage valid observations over time for the period January 2007 – December 2008, based on the global MERIS based output of P-model GPP.

4.3. Global EO intercomparison

In this chapter the dataset of global P-model GPP images are compared against two other EO products: Copernicus DMP and MODIS GPP. The comparisons are done in a number of ways with each having their own focus.

4.3.1. Spatial distribution of the GPP estimates

In this analysis, we want to highlight spatial patterns or hot spots of agreement or disagreement between the P-model GPP and the EO benchmark data. For this, statistical measures are derived from the per pixel time series that estimate the percentage of systematic and unsystematic differences (see 3.2).

Systematic differences between the P-model and the Copernicus GPP are mostly situated in the upper northern regions and around the tropics. In the comparison with MODIS, also in the northern regions, disagreements are mainly caused due to systematic differences. But in the tropic area, the differences are mainly unsystematic.

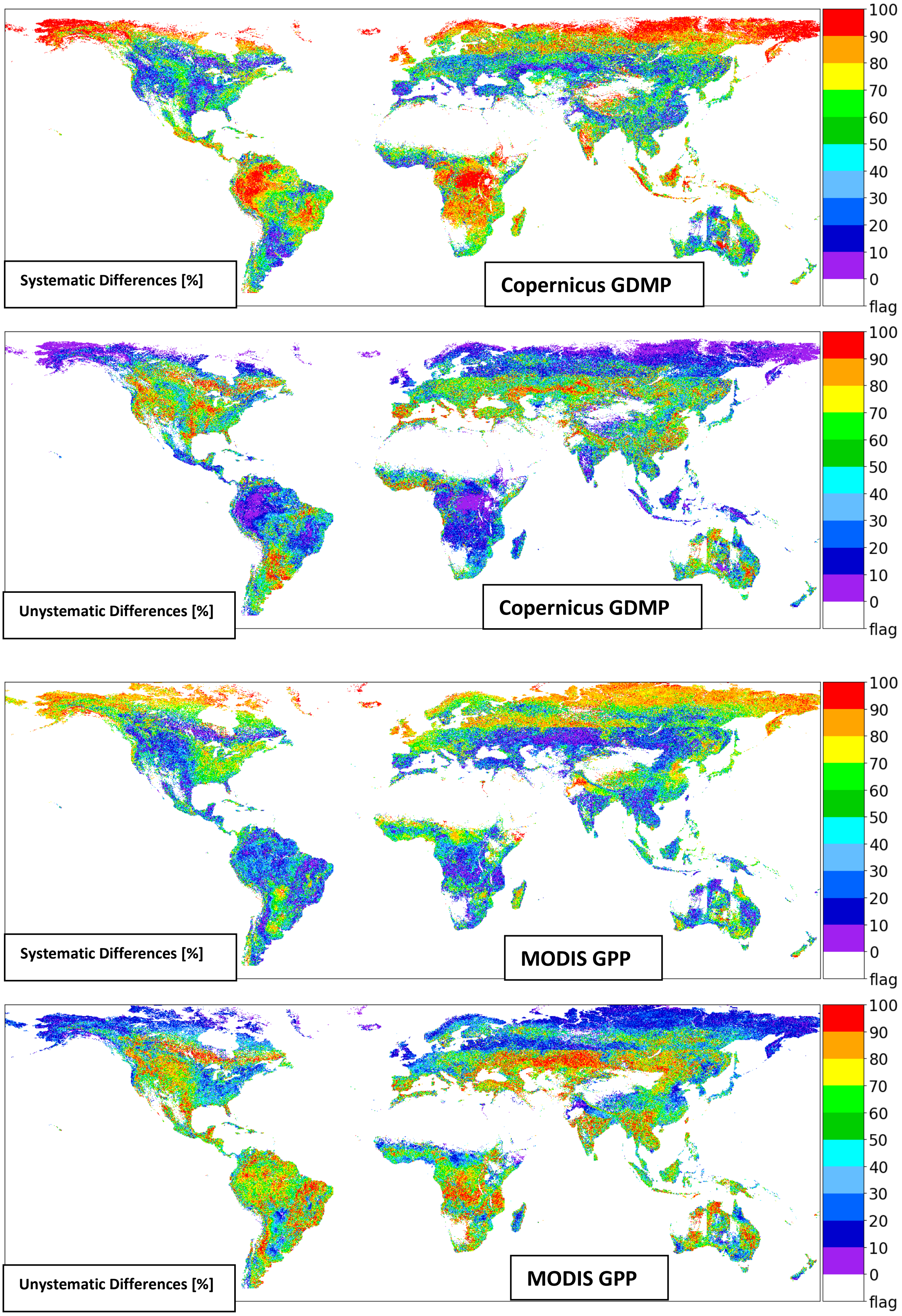

Figure 11: Systematic and unsystematic differences in the global time series compariso of the P-model GPP and Copernicus and MODIS GPP.

4.3.2. Histograms

In this chapter, the global P-model frequency distribution of the GPP values are analyzed per biome, based on a modified CCI land cover classification. Resulting histograms are compared with the Copernicus GDMP (Figure 12) and MODIS (Figure 13). This is done per biome, based on a modified CCI land cover classification and for all land pixels. In the analyses, only pair-wise pixels are included which have a valid GPP value for both datasets.
For all land covers, the P-model estimates have less close-to-zero values than the Copernicus. This is the same in the MODIS comparisons. For higher productive cropland (>5 gC/m2/day), assumably when crops are in their growing season, the P-model has lower values then Copernicus, but higher values then MODIS. For broadleaved evergreen forests, the distributions are fairly different amongst the datasets. The P-model has mostly lower values then Copernicus, and higher then MODIS.

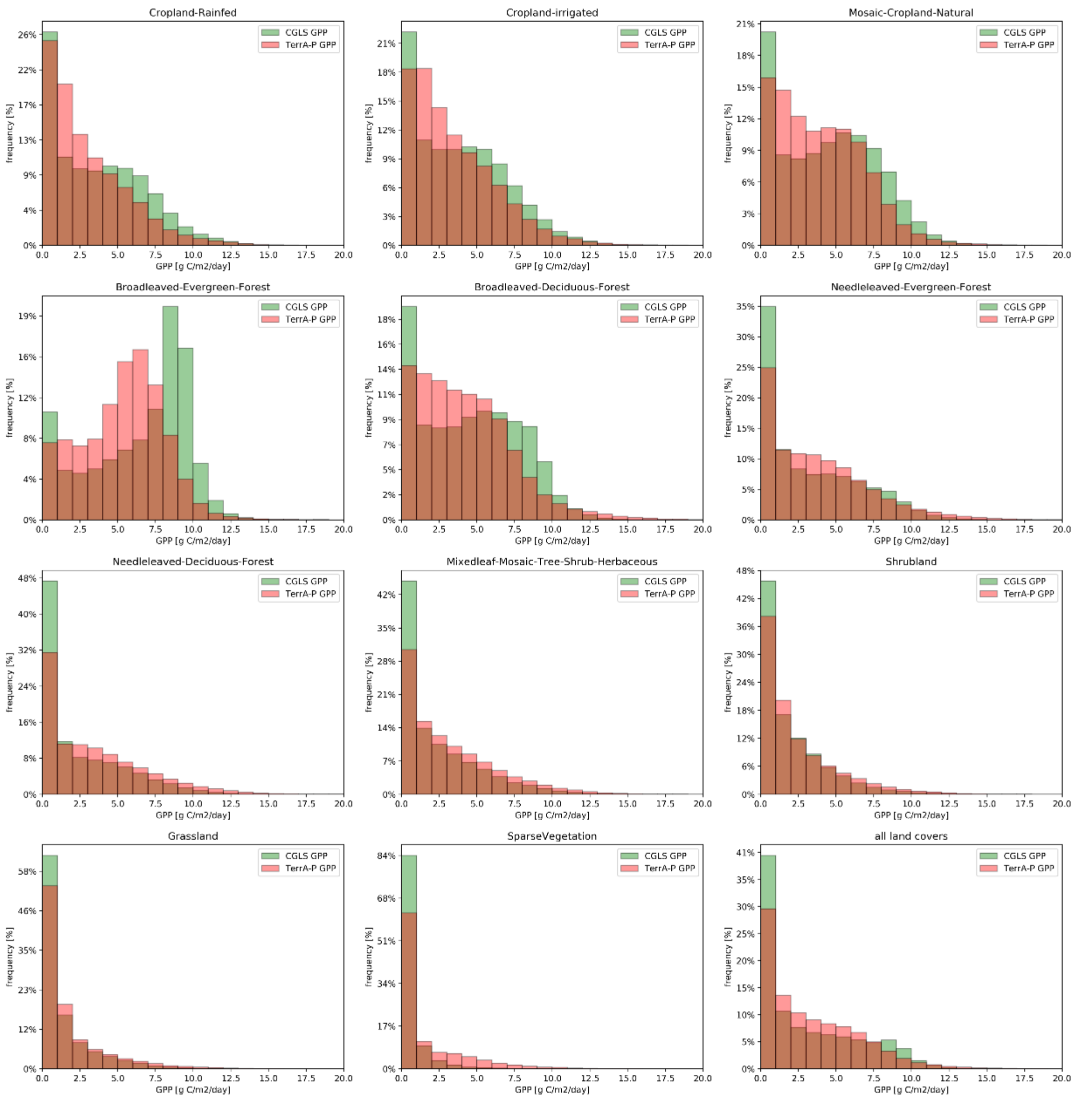

Figure 12: Histograms of the global frequency distribution of the GPP values derived from P-model estimates and compared against the Copernicus GDMP (scaled to GPP).

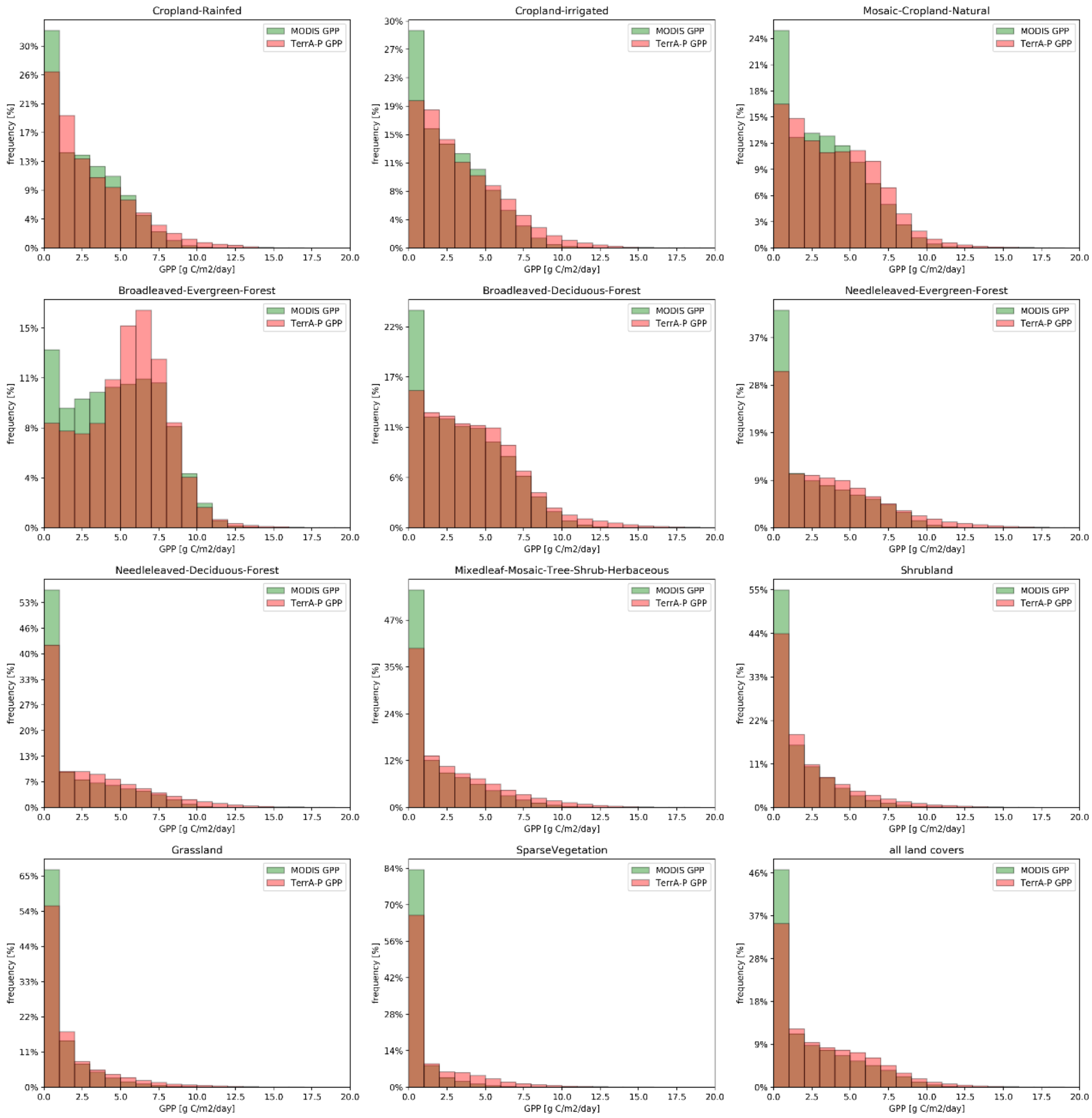

Figure 13: Histograms of the global frequency distribution of the GPP values derived from P-model estimates and compared against the MODIS GPP.

4.3.3. SCATTERPLOTS

In this section, GPP values of the P-model are pixel wise compared against Copernicus and MODIS. All observations over the two year period are aggregated per land cover and plotted in a scatter density plot. The Geometric Mean Regression and R squared are calculated per analysis. Some general findings:

- The general relation for most land covers is fairly strong (R squared >0.6) but a large scatter is visible on all plots.
- The P-model has a certain part of high values (GPP>15 g C/m2/day) which are not present in the other two datasets. Remark: MODIS values are topped off at 15 g C/m2/day due to a rescaling. But the fraction of >15 gC/m2/day GPP is negligible.
- For very low values (<1 gC/m2/day), the P-model has mostly higher values then the other two datasets.
- There is also a general positive bias of P-model over sparsely vegetated areas.

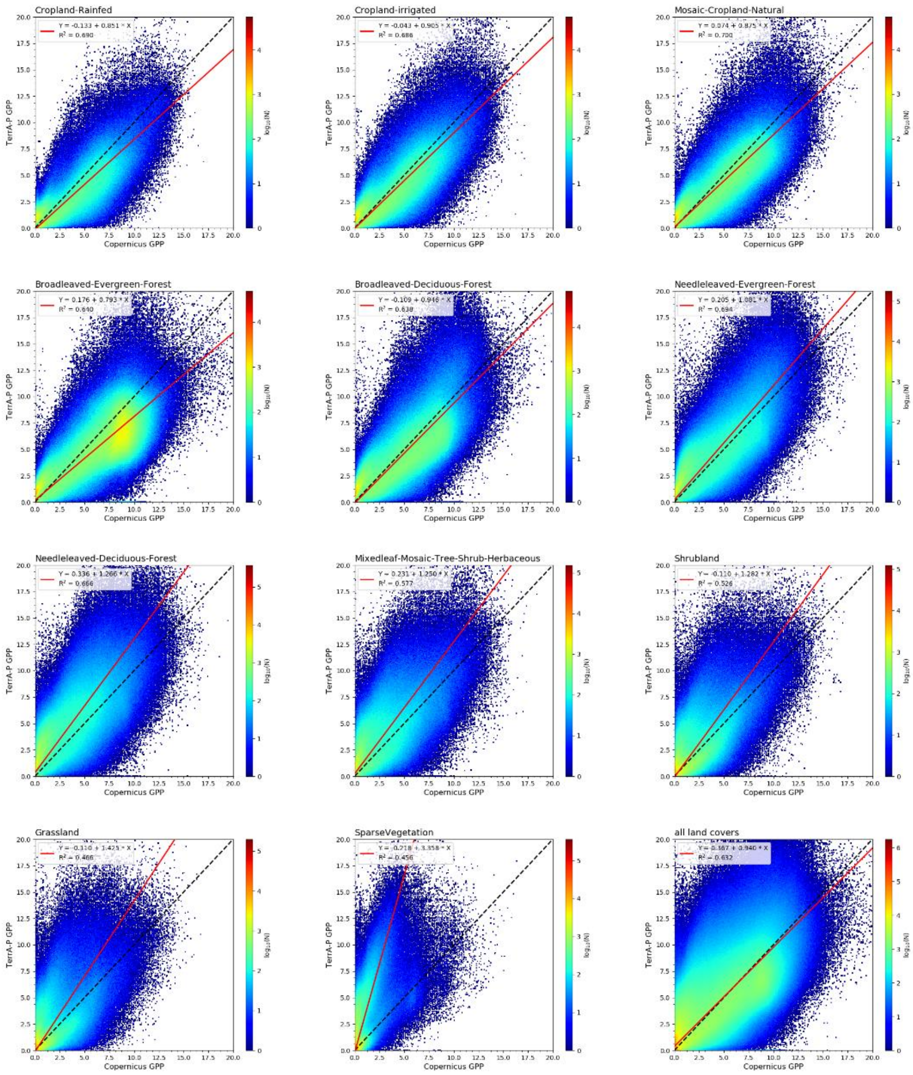

Figure 14: Density scatterplots of the GPP values derived from the P-model and Copernicus estimates, globally per land cover, over the dekadal time series 2007-2008.

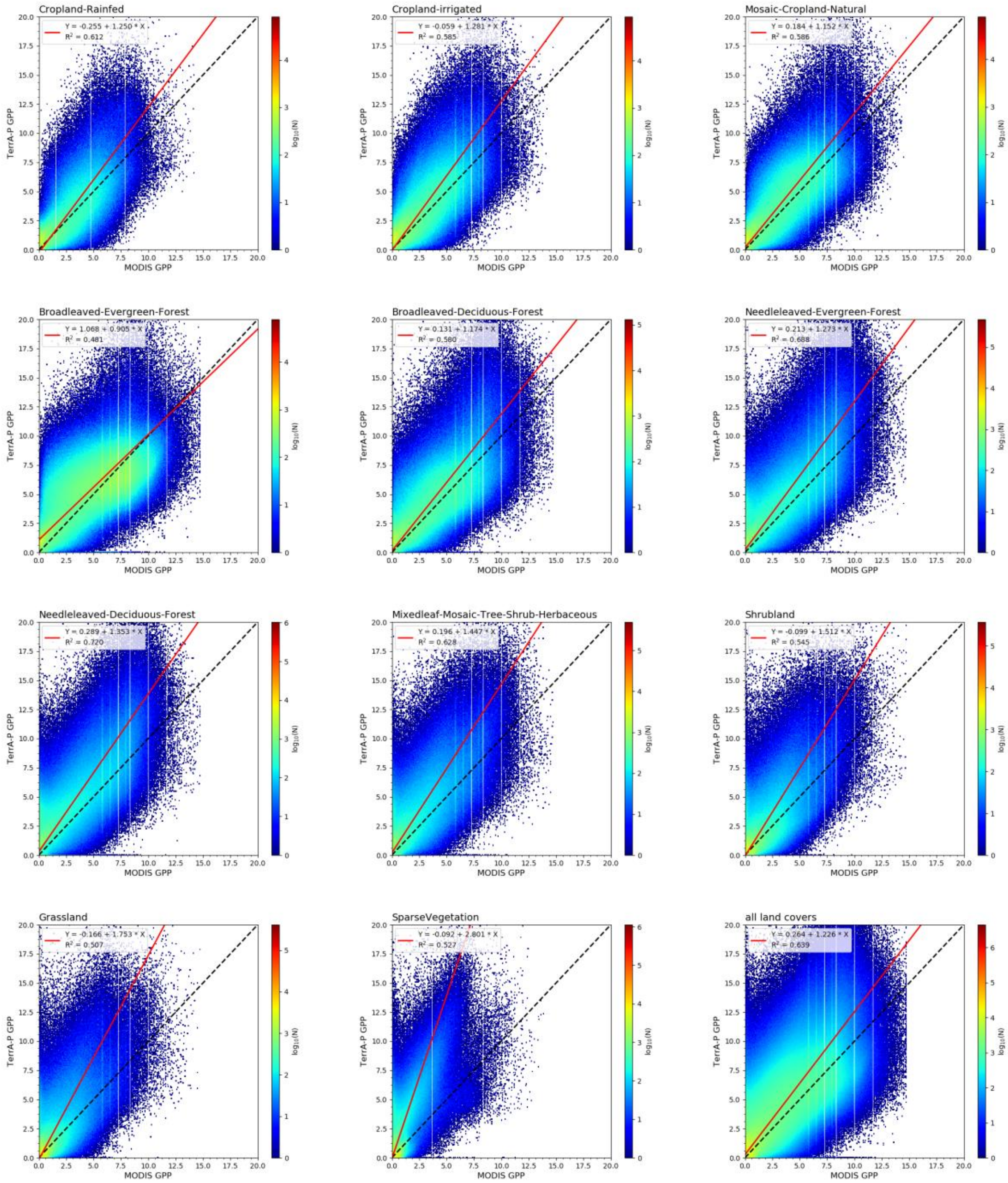

Figure 15: Density scatterplots of the GPP values derived from the P-model and MODIS estimates, globally per land cover, over the dekadal time series 2007-2008.

4.3.4. TEMPORAL VARIATION PER REGION & BIOME

In this chapter the general temporal behavior of the different GPP estimations are analyzed for different biomes and regions. For the biomes, the CCI land cover is used. The regions are derived from the UN's GAUL (Global Administrative Unit Layer). In annex, all graphs are shown. In this chapter, we illustrate some of our findings with a selection of the graphs. General findings are given per continent, but the most relevant intercontinental differences are also described.

→ Africa

For most of the biomes over all Africa (Figure 16), the P-model GPP is in agreement with MODIS. The Copernicus values are systematically lower then the other two dataset. Looking in more detail, it appears that this is indeed the case for the separate regions in Africa. Only for Western Africa (Figure 18) the situation is different. Here, the P-model GPP is similar to its Copernicus variant and both are higher then MODIS.

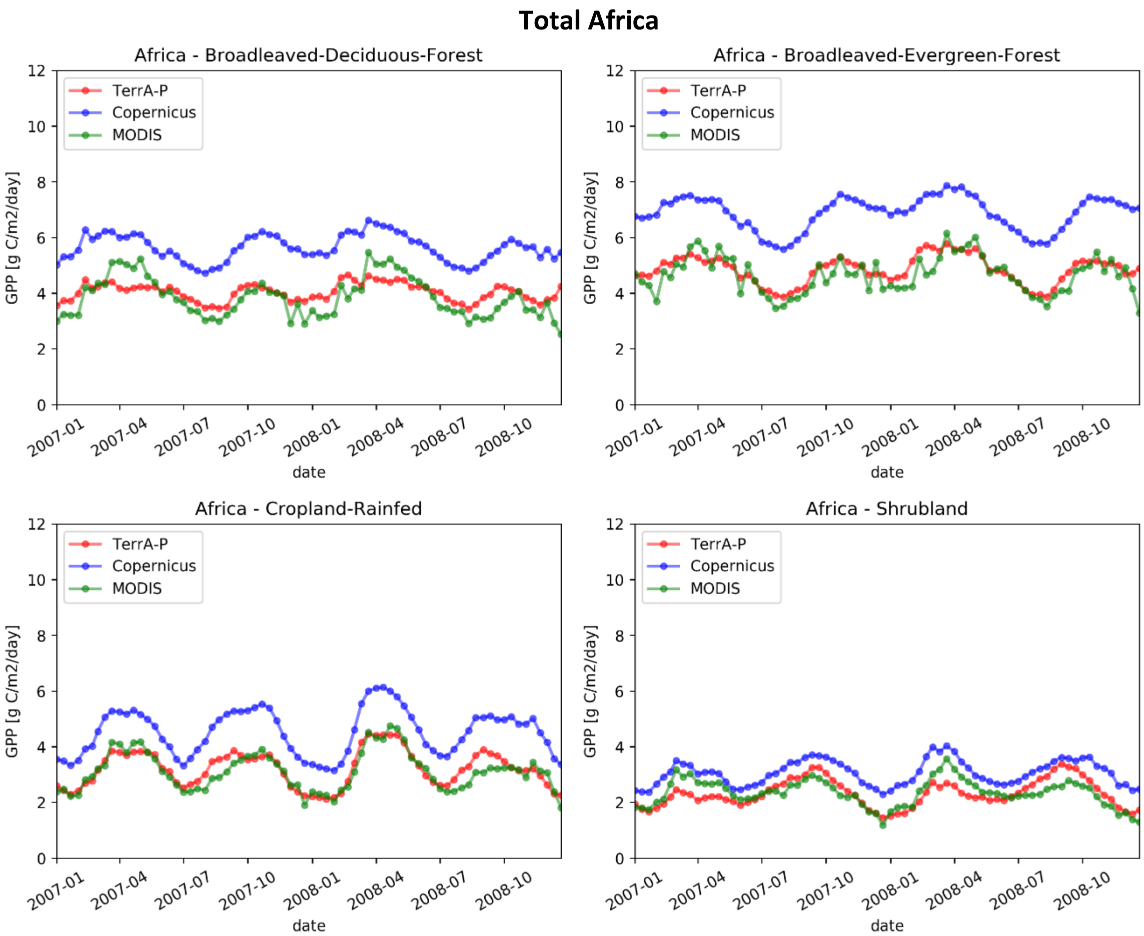

Figure 17: Regional GPP averages for different biomes in Africa for the P-model, Copernicus GDMP and MODIS.

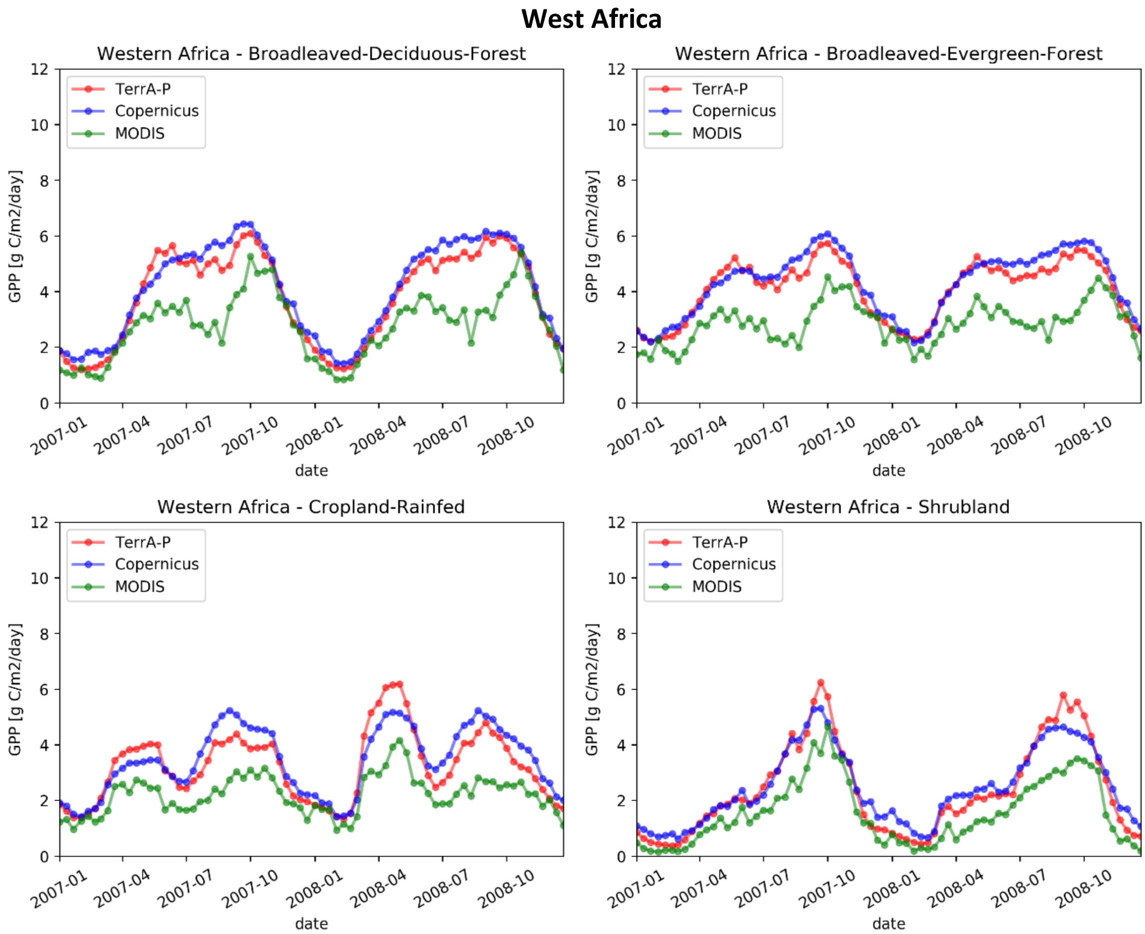

Figure 18: Regional GPP averages for different biomes in West Africa for the P-model, Copernicus GDMP and MODIS.

→ Americas

In this analyses, we 've split up the result for North, Central and South America.
In ***Northern America*** (Figure 19), the P-model GPP is very alike to the Copernicus GPP for the forest and cropland biomes. It seems however that the P-model tends to have an earlier onset of the growing season. For grassland and shrubland, P-model has higher estimates then Copernicus and MODIS.

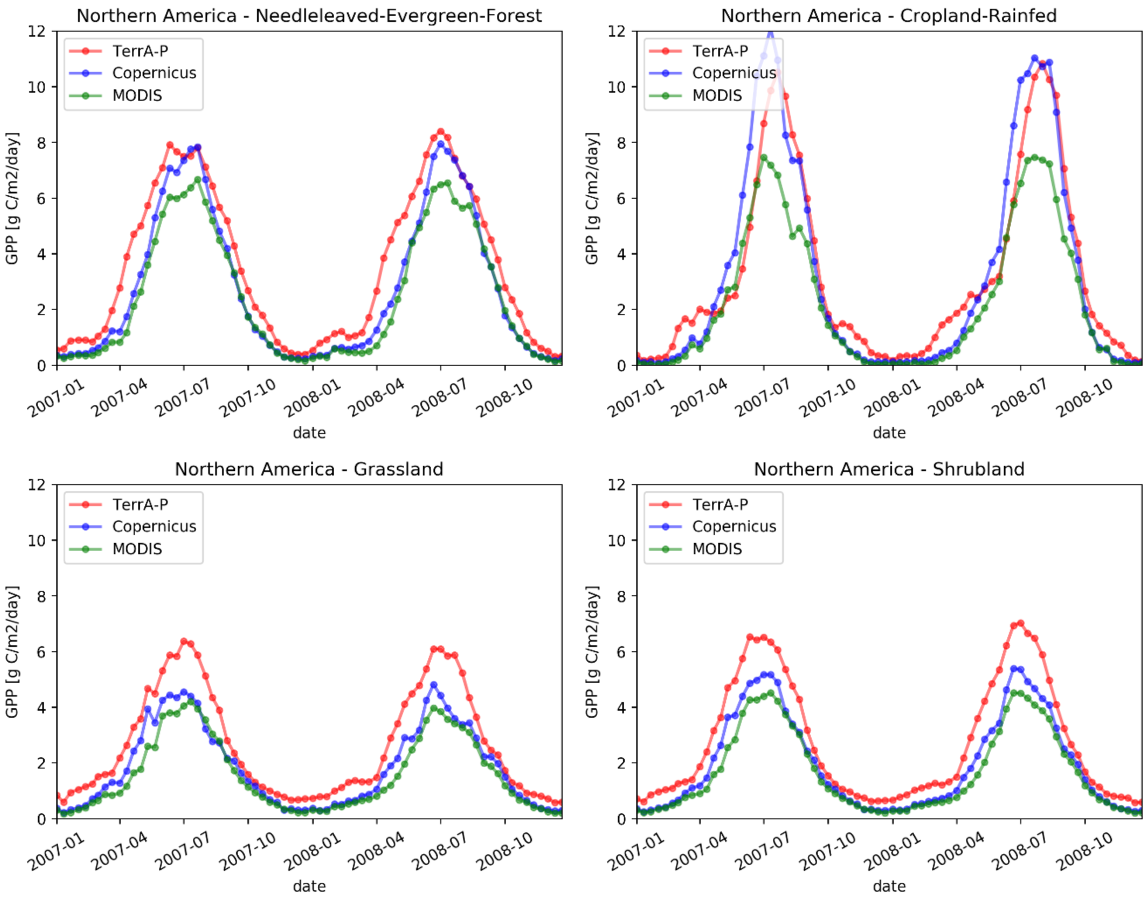

Figure 19: Regional GPP averages for different biomes in Northern America for the P-model, Copernicus GDMP and MODIS.

In ***Southern America*** (Figure 20), the P-model temporal GPP profiles have a similar phenology then the Copernicus data for broadleaved deciduous and broadleaved evergreen forests. However, there is a systematic difference. The MODIS time series regarding magnitude more in line with the P-model, but doesn't show the same seasonal pattern and is less smooth over time. For Cropland, the P-model is line with MODIS but with a higher peak. Copernicus shows an earlier onset of the season and higher GPP values throughout the growing season. For shrubland, the three datasets have a similar pattern, but Copernicus is higher then the other two datasets.

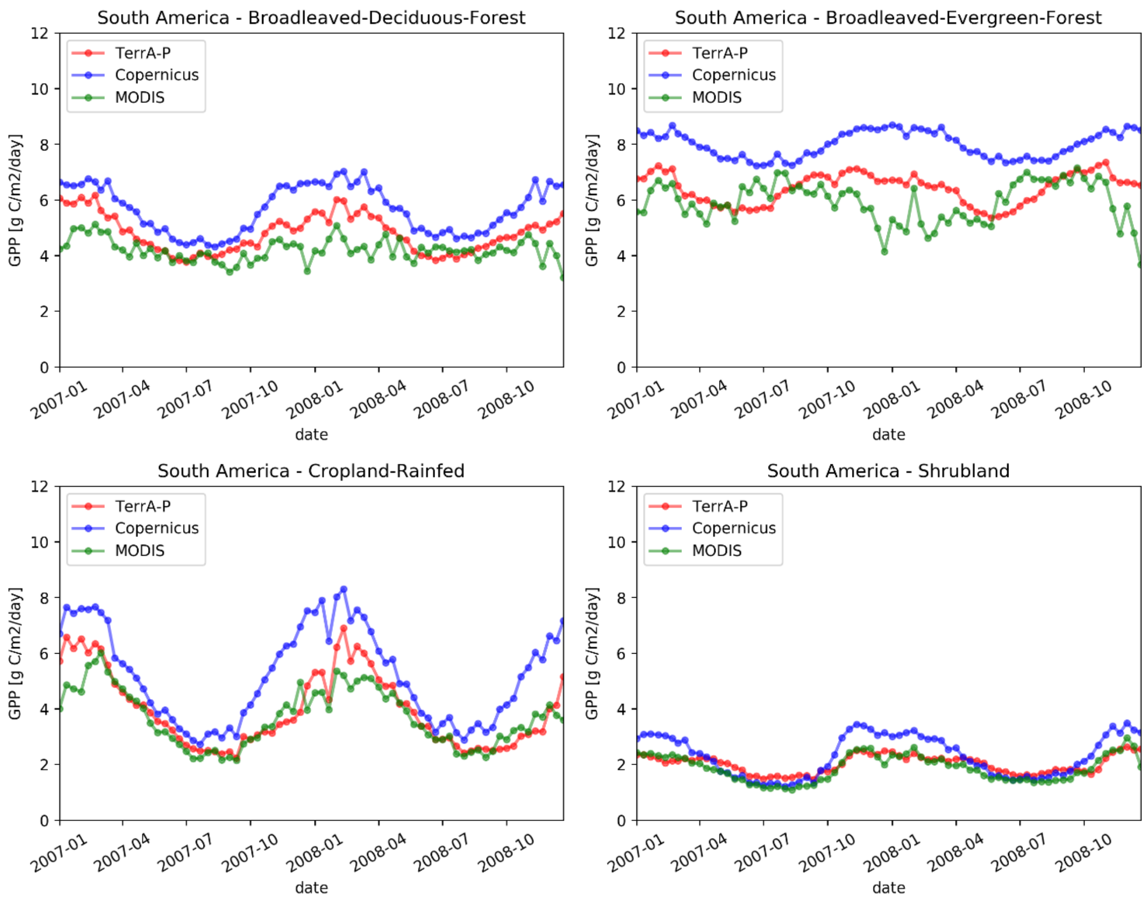

Figure 20: Regional GPP averages for different biomes in Southern America for the P-model, Copernicus GDMP and MODIS.

→ Europe

The P-model GPP's for ***needleleaved forests*** (both deciduous and needleleaved, Figure 21) are higher than MODIS and Copernicus for most of the European continent. Only in southern Europe (Figure 22), the mediterenean pine forests are estimated rather similar for the three datasets, with a slightly higher values for Copernicus.

Europe – needleleaved forests

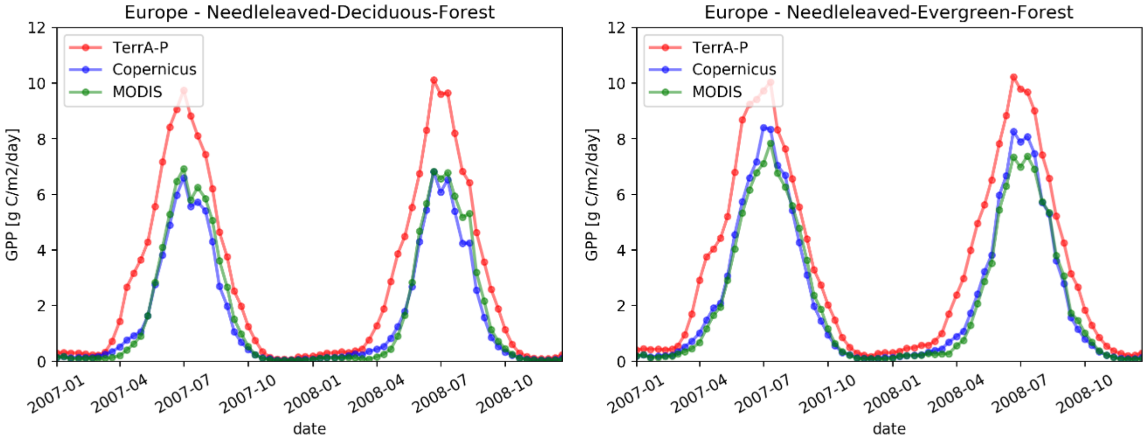

Figure 21: Regional GPP averages for needleleaved forests in Europe for the P-model, Copernicus GDMP and MODIS.

Southern Europe – needleleaved forests

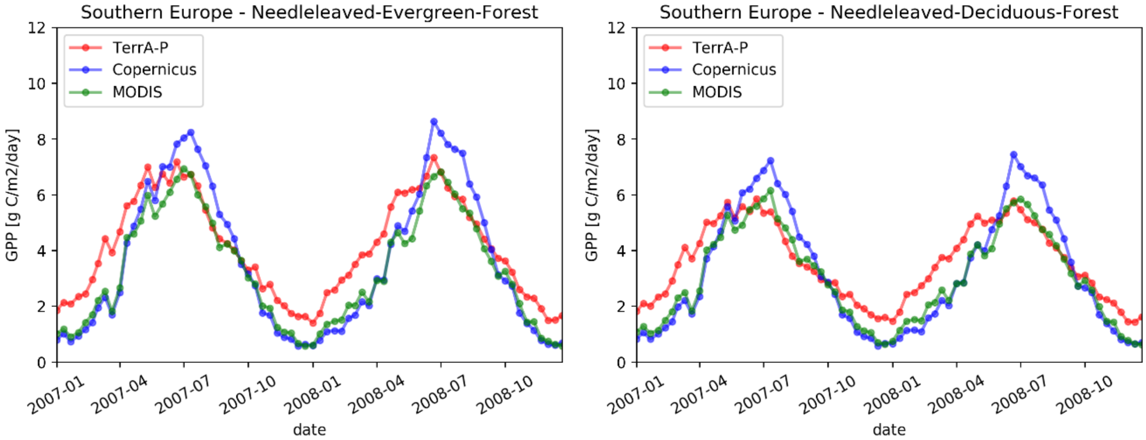

Figure 22: Regional GPP averages for needleleaved forests in Southern Europe for the P-model, Copernicus GDMP and MODIS.

Europe - Broadleaved Deciduous forests

Broadleaved deciduous forests have a similar order of magnitude of the estimated GPP at the peak of the growing season in Western and Southern Europe (Figure 23). In Northern and Eastern Europe, the P-model estimates are higher. The phenology of the season is also slightly different for the P-model, with an earlier onset and a somewhat later end of the growing season.

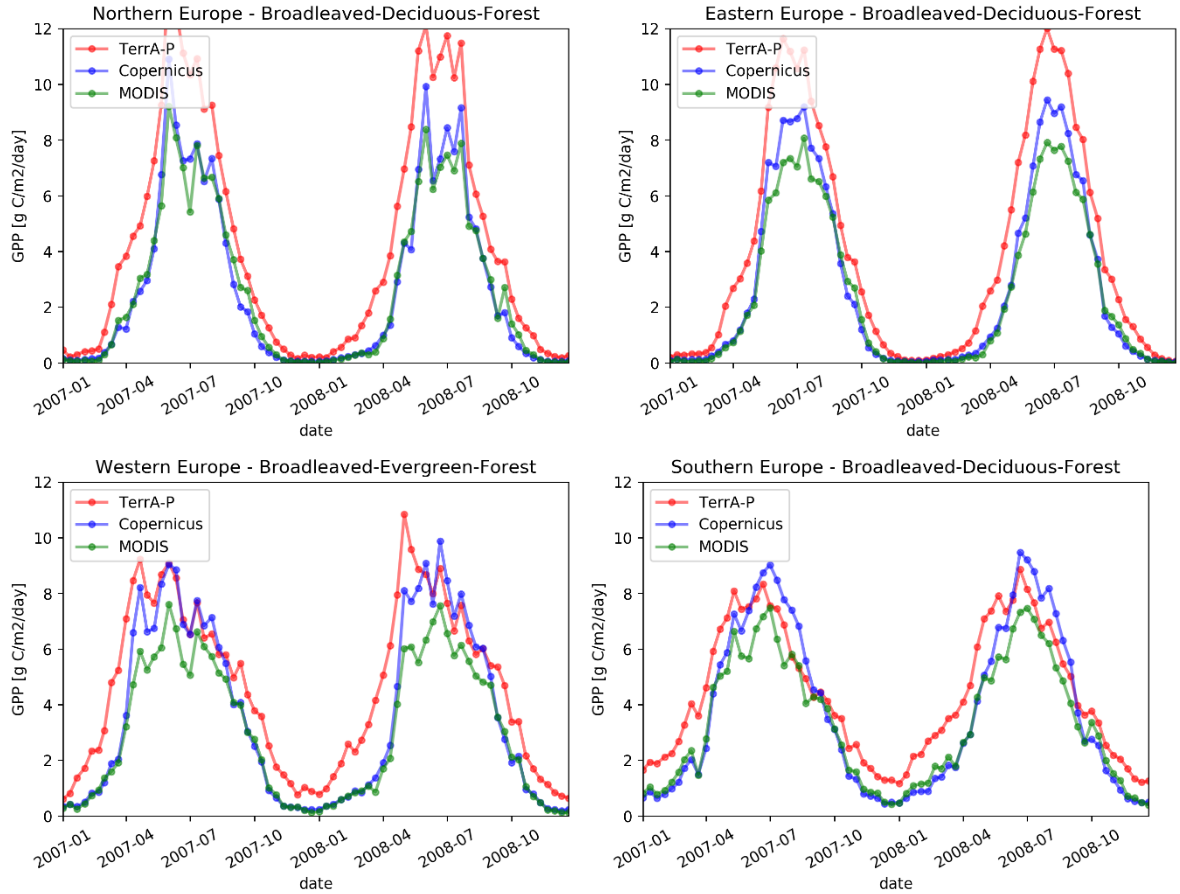

Figure 23: Regional GPP averages for broadleaved deciduous forests in different regions in Europe for the P-model, Copernicus GDMP and MODIS.

Europe – Cropland

In most parts of Europe, similar patterns are found for cropland (Figure 24). The onset of the seasons is somewhat earlier for the P-model GPP as compared to the two other datasets. This is also observed in other land covers and biomes. The Copernicus reaches the highest GPP values at the peak of the season. For rainfed cropland, the P-model peak GPP's are comparable to MODIS, but for irrigated cropland, the P-model GPP's are higher then MODIS. In southern Europe (Figure 25), the cropland phenology of the P-model is different from the other two datasets, especially for rainfed cropland. The onset and peak are earlier, and the productivity drops fast after May/June.

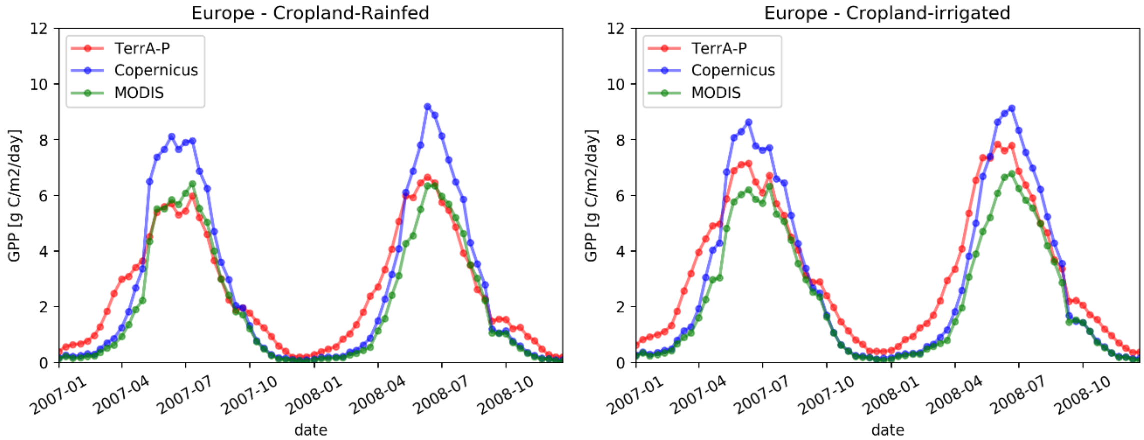

Figure 24: Regional GPP averages for cropland in Europe for the P-model, Copernicus GDMP and MODIS.

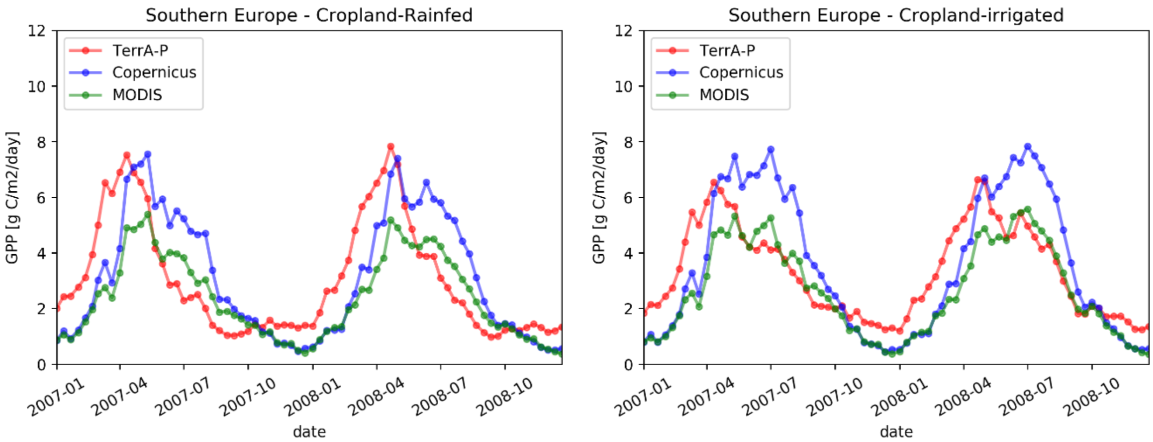

Figure 25: Regional GPP averages for cropland in Southern Europe for the P-model, Copernicus GDMP and MODIS.

Europe – Shrubland & Grasslands

In Northern and Eastern Europe (Figure 26), the P-model GPP is significantly higher throughout the growing season for grassland and shrubland then Copernicus and MODIS. In southern Europe, they are quite similar, the P-model is even a bit lower in the growing season. In Western Europe, the P-model has slightly higher estimates for grassland and shrubland. The onset of the season is generally earlier in the P-model than the other two products.

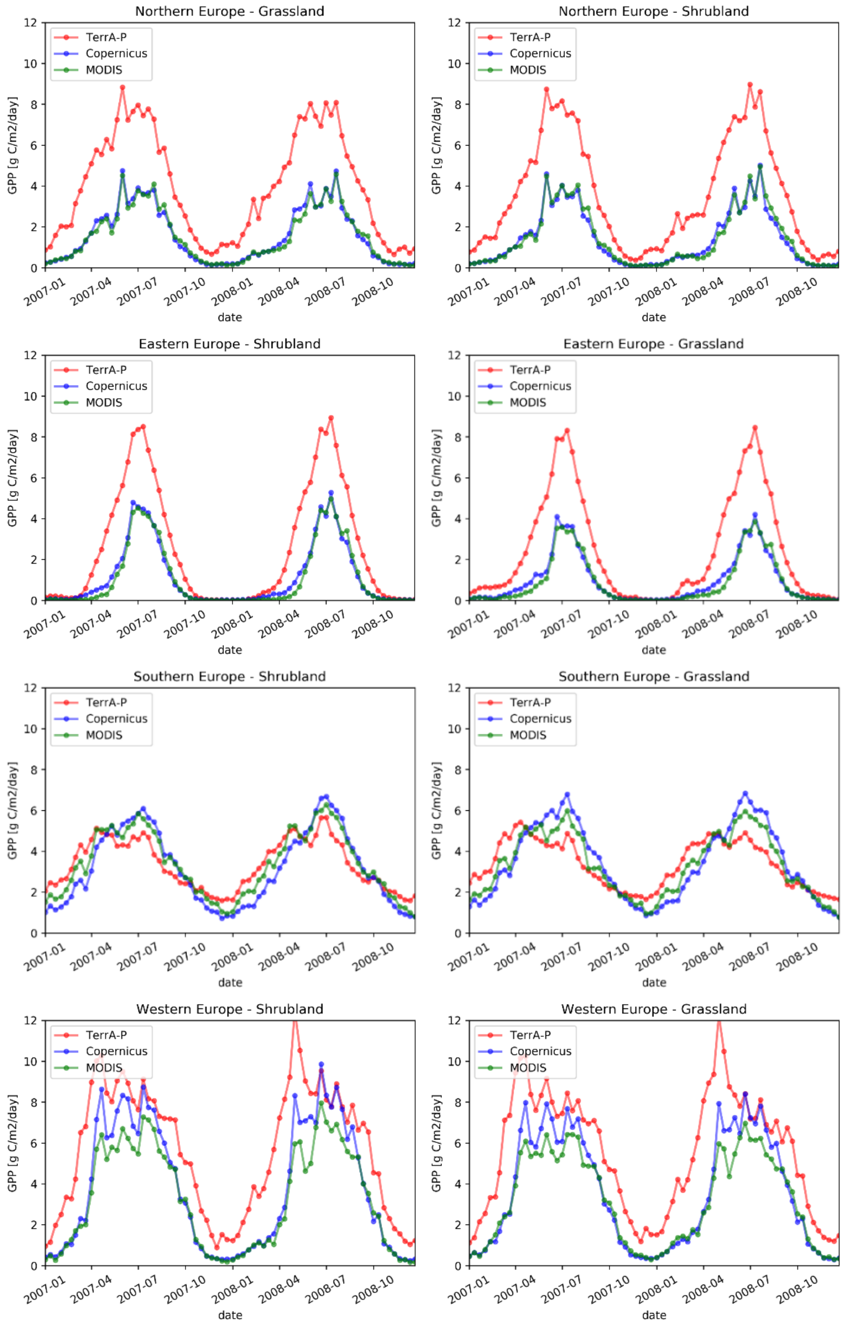

Figure 26: Regional GPP averages for shrubland and grassland in different regions in Europe for the P-model, Copernicus GDMP and MODIS.

→ Asia

In Asia (Figure 27), the P-model GPP for cropland has a higher peak then MODIS but is lower then Copernicus. The broadleaved deciduous forest GPP is fairly similar to the Copernicus GPP, MODIS has a much lower magnitude of the growing season peak values. For grassland, the P-model GPP has an earlier onset of the season and lower magnitude of the values than the other two datasets. For broadleaved evergreen forests, the P-model is just in between the Copernicus and MODIS GPP. For needleleaved evergreen forests, the TerrA-P GPP has an earlier onset and higher values then MODIS but lower then Copernicus.

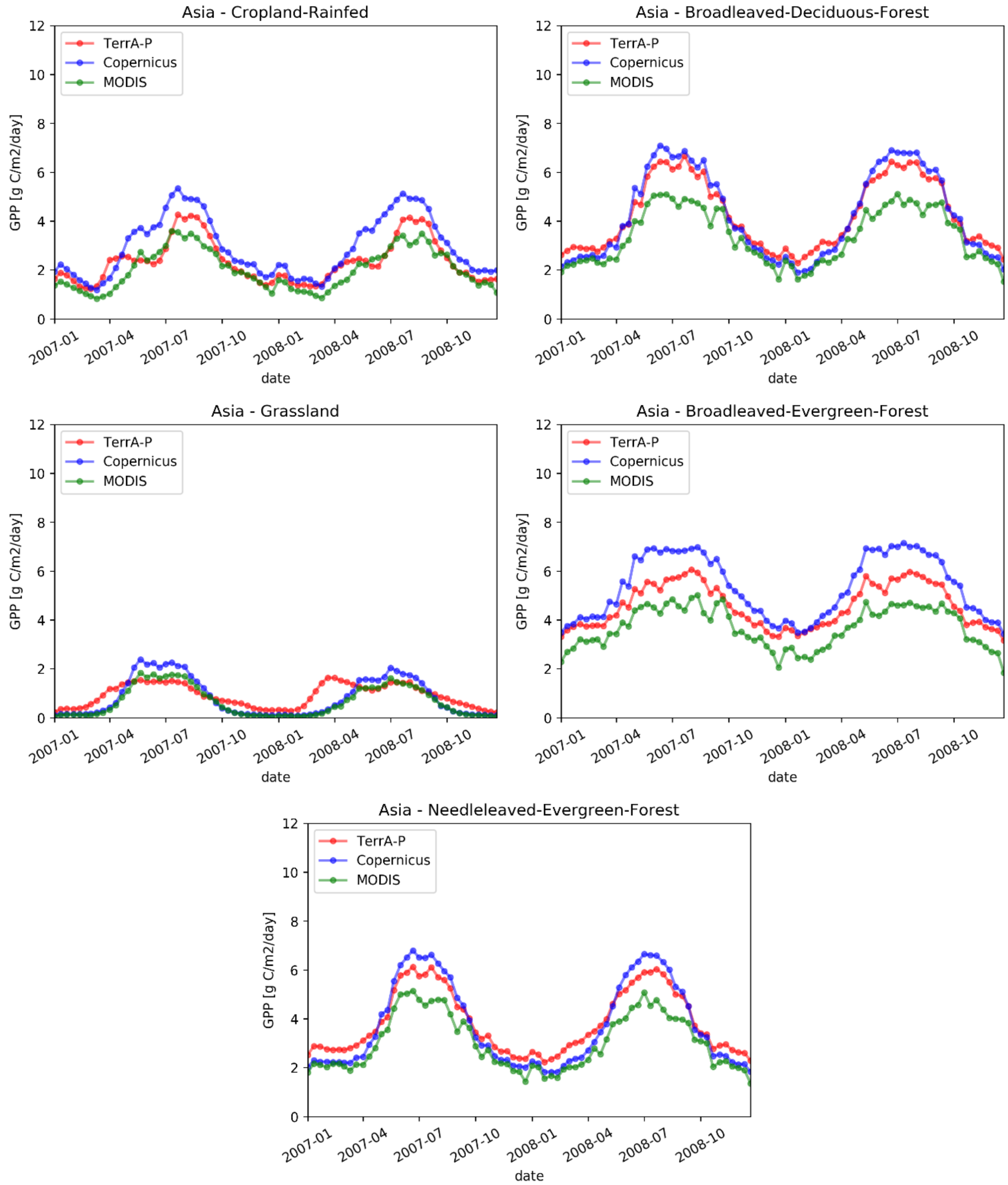

Figure 27: Regional GPP averages for five land covers in Asia for the P-model, Copernicus GDMP and MODIS.

4.4. LOCAL ACCURACY ASSESSMENT

In this chapter, the GPP estimations for the three EO dataset are compared against in-situ GPP values derived from FLUXNET towers for the years 2007-2008.

General assessment

The TerrA-P GPP values are generally slightly higher then the FLUXNET estimates, with a regression line slope of 1.07 and an offset of 0.46 g C/m2/day. The RMSE is 2.59 g C/m2/day as compared to 2.18 for Copernicus GPP and 2.30 for MODIS. All proldučts match the FLUXNET data fairly well, which could be explained by the fact that they all use FLUXNET data in their calibration. MODIS slightly underestimates FLUXNET, which could be related to the exclusion of a CO_2 fertilization factor. It remains to be investigated why the TerrA-P slightly overestimates the FLUXNET data.

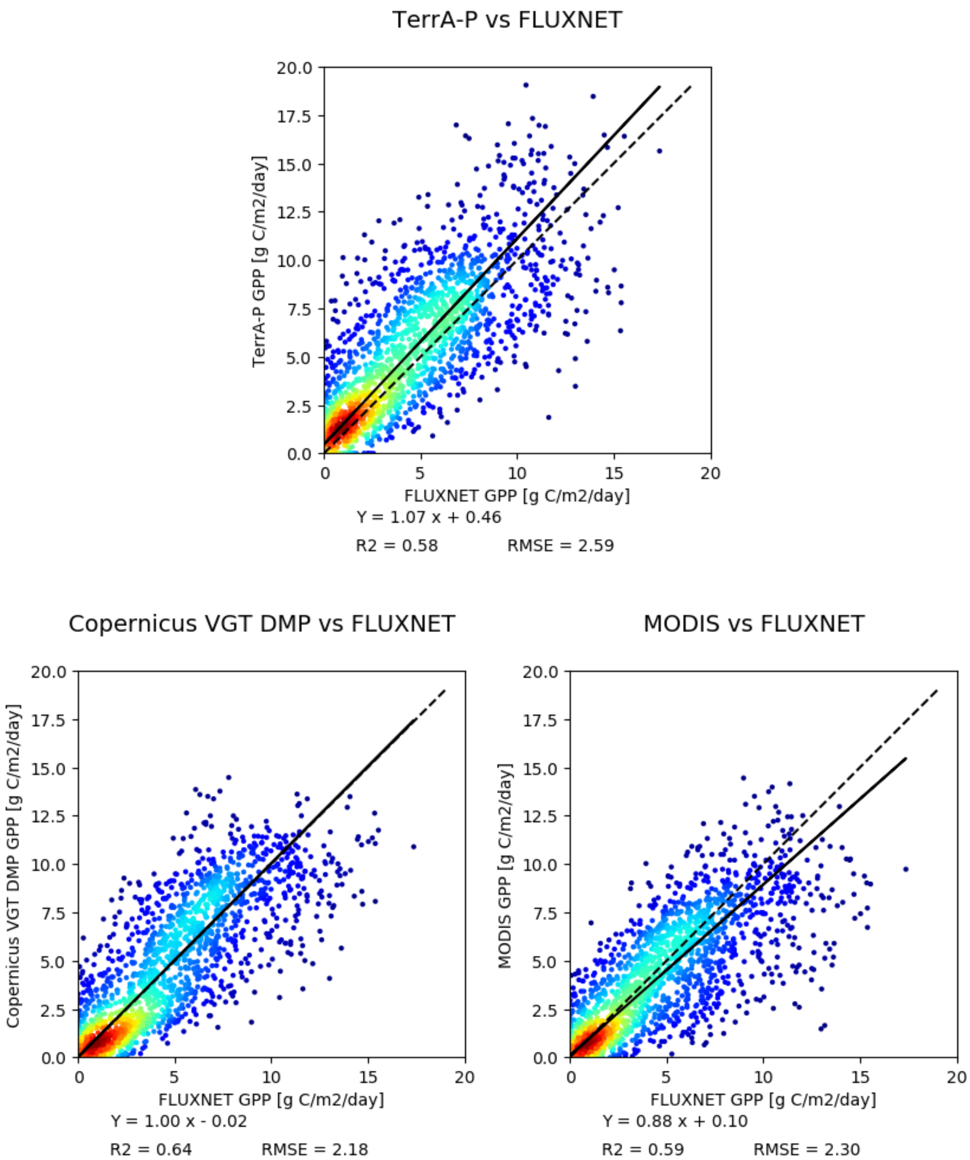

Figure 28: 10-daily GPP of three different EO based GPP models versus in-situ GPP values derived from FLUXNET towers for the years 2007 – 2008.

CHAPTER 5 CONCLUSIONS

This report summarizes the generation and evaluation of a global P-model based GPP (& uncertainties) test dataset for the years 2007 & 2008. The inputs for the model were:

- fAPAR (or GVI) derived from ENVISAT MERIS
- LST derived from ENVISAT AATSR
- Incoming Radiation & Vapour Pressur derived from ECWMF

All input and output datasets are standardized to a 10-daily 1 km global grid.

Below, some conclusions on different components of the global P-model dataset generation, evaluating and benchmarking with other EO models:

Product requirements

- The global test dataset meets the temporal and spatial dimensions of the product requirements, which are 10-daily 1 km global images.

Preparation of global EO input datasets

- The original 10-daily input fAPAR data is still perturbated by outliers and missing data points, e.g. due to clouds and shadows. During the point level GPP model developments (a priori to the global implementation), it was chosen to smooth the time series of fAPAR to eliminate such outliers and to obtain a continuous time series. For the global implementation, this approach was followed.
- For the global LST data, the coverage was insufficient to yield a robuste 10-daily global time series. Hence also a smoothing and gap filling procedure was applied.
- For the fAPAR no uncertainties were available. For LST, uncertainties were available for the original observations. But it is still unclear how these should be propagated to a 10-daily smoothed and gap-filled product. Hence, no per-pixel input uncertainties were used as inputs in the model.

Global P-model implementation

- The original P-model code was completely revised. In the new code, two Python files are needed to run the model: a Python script to initiate the uncertainty calculations and one containing the entire algorithm, split into functions. There is now one global function that requires equally sized input arrays for fAPAR, LST and meteo-data (and possible uncertainties) and provides as output a GPP and GPP uncertainty array. This code will be put online on a public GIT repository.
- The model runs quite efficiently as it uses Python Numpy array calculations. The systematically thinned (21x21km) dataset can be processed on a local laptop. The global 1 km processing chain would require too much memory and is hence operated in a parallel processing chain on VITO's processing clusters.
- Orginally two versions of the P-model are available: a C3 and C4 model. But in this global implementation, only C3 outputs are generated.

Global P-model outputs – general findings

- Generally, the model outputs seem reasonable and agree to the expected behavior of the model.
- There are cases when the model provides GPP outputs when no uncertainties are estimated, or the opposite way. This will be further investigated.
- The model fails to provide GPP values (“no_data”) for sparsely vegetated areas, e.g. inner Australia (January/October), Sahel (April), Great Basin – US (July),…
    - This is probably caused by too high LST values. In sparsely vegetated areas, the LST estimates are largely based on soil temperatures, rather then on vegetation canopy temperatures. This can result in extreme values (>45°C) which cause the P-model to produce model errors as it can’t deal with these extremes. This is currently one of the major challenges when using LST data in the model temperature component. There is no direct solution for this. These spatial pattern match also the distribution of vegetation dominated byC4 plants, operate at far higher leaf temperatures, up to about 60˚C. So a possible solution could be to run a C4 model where needed.
- There seems to be an artificial horizontal boundary in the northern regions in the April map. This is further propagated from the LST maps.

Global P-model outputs – comparison with other EO data

- Overall, TerrA-P predictions are generally quite close to MODIS and Copernicus. They are quite often in between MODIS (lower) and Copernicus (higher).
- Below some of the model specific clarifications:
    - The P-model GPP has generally a higher fraction of very low values (< 0.7 gC/m2/day) then the other to products. This could be related to the temperature response function. It is probably because the low-temperature response of the instrinsic quantum efficiency ϕ_0 in the P model (in the version used here) is extremely simple, i.e. it is a step function, with value zero when temperature falls to or below zero, but no gradual inhibition with temperatures lower than +- 15˚C. Recent insights shows that ϕ_0 actually does decline gradually with low temperatures. Recently, an updated version of the P-model is developed with a specific (observationally based) function for this effect, in C3 plants, and another one for C4 plants. It is however not used in this assessment. MODIS and Copernicus probably mimics this effect by using an optimum curve for photosynthesis. In this respect, therefore, we guess that TerrA-P is underestimating the low values.
    - The above issue could be responsible for the most consistent cases of disagreement in the seasonal cycles of GPP between TerrA-P and the other two models. These are mainly in evergreen vegetation (e.g. ENF and grasslands) at high latitudes. The leaves are still green, and there is some light, even when temperatures is these regions – such as N and E Europe – are low enough (approaching but not equalling zero) to reduce ϕ_0. This also could explain the earlier onset of the season of the P-model as compared to MODIS and Copernicus.

- Finally, by far the largest differences between TerrA-P and the other two models are for sparse vegetation where, in general, it seems that TerrA-P produces several times higher GPP. Here, we suspect that TerrA-P is right, and that the other models reduce photosynthesis too much at moderately high temperatures. This is a common problem in ecosystem models generally.

LIST OF LITERATURE

Eilers, P.H.C., 2003, A perfect smoother. Analytical Chemistry, 75, pp. 3299–3304.

Heinsch, F.A., et al. (2003). User's Guide GPP and NPP (MOD17A2/A3) Products NASA MODIS Land Algorithm.

Keenan, T.F., I.C. Prentice, J.G. Canadell, C. Williams, H. Wang, M.R. Raupach and G.J. Collatz (2016) Recent pause in the growth rate of atmospheric CO2 due to enhanced terrestrial uptake. Nature Communications 7: 13428.

Montheith, L.J. (1972). Solar Radiation and Productivity in Tropical Ecosystems. The Journal of Applied Ecology, 9(3), pp.747–766.

Running, S. et al. (1999). MODIS daily photosynthesis (PSN) and annual net primary production (NPP) product (MOD17). Algorithm Theoretical Basis Document, Version 3.0, (29 April), pp.1–59.

Swets, D. L., B. C. Reed, J. D. Rowland, and S. E. Marko. 1999. "A Weighted Least-Squares Approach to Temporal NDVI Smoothing." In: Proceedings of the 1999 ASPRS Annual Conference, 526–536. Portland, OR.

Swinnen et al. (2018). Gio Global Land Component - Lot I "Operation of the Global Land Component". Algorithm theoretical basis document. Dry Matter Productivity (DMP). Version 2, Issue 2.10, online at https://land.copernicus.eu/global/sites/cgls.vito.be/files/products/GIOGL1_ATBD_DMP1km-V2_I2.10.pdf

Verger, A., Baret , F., & Weiss, M. (2008). Performances of neural networks for deriving LAI estimates from existing CYCLOPES and MODIS products. Remote Sensing of Environment, 112, 2789-2803

Wang, H., I.C Prentice, W.M. Cornwell, T.F. Keenan, T.W. Davis, I.J. Wright, B.J. Evans and C. Peng (2016a) A universal model for carbon dioxide uptake by plants. bioRxiv http://dx.doi.org/10.1101/040246 (preprint; revised version in revision for Nature Plants).

Wang, H., I.C. Prentice, T.W. Davis, T.F. Keenan, I.J. Wright and C. Peng (2016b) Photosynthetic responses to altitude: an explanation based on optimality principles. New Phytologist 213: 976–982.

Zhao, M. et al. (2005). Improvements of the MODIS terrestrial gross and net primary production global data set. Remote Sensing of Environment, 95(2), pp.164–176.